FACULTY OF SCIENCE AND TECHNOLOGY

MASTER THESIS

Study programme / specialisation: Petroleum Technology / Reservoir Engineering	The spring semester, 20..... Open / Confidential
Author: Johan Helgø	..... (signature author)
Course coordinator: Pål Østebø Andersen Supervisor(s): Pål Østebø Andersen, Solveig Riisøen	
Thesis title: Reservoir simulation of measurements with an innovative tool to detect oil-water-contact	
Credits (ECTS): 30	
Keywords: Capillary Pressure, Simulations, Free Water Level,	Pages: .....48..... + appendix: ..... Stavanger, ... date/year

Reservoir simulation of measurements with an innovative tool to detect oil-water-contact

---

Master Thesis by
Johan Helgø (232546)

Universitetet
i Stavanger

Spring 2022

Department of Energy Resources

Acknowledgments

This thesis «Reservoir simulation of measurements with an innovative tool to detect oil-water-contact» was created by Solveig Riisøen (Hydrotell) for Department of Energy Resources at the University of Stavanger and written by Johan Helgø. Helgø would like to thank Riisøen for the opportunity to be a part of this project and for valuable input underway. Thank you to Pål Ø. Andersen for being an endless source of input during the process.
A special thanks is given to Arild Lohne at Norce Research Center for input on IORCoreSim and Berea core sample data.

It must be pointed out that the tool in question is in the making by Hydrotell and have thus not been tested in a real-life reservoir. Thus, it is hard to say if the tool would produce the results given in this thesis. This thesis is not attempting to predict what the tool will measure, only to predict what the tool should measure. Views expressed in this thesis belong to Johan Helgø alone.

Abstract

Hydrotell is developing a tool which will measure the pressure difference between oil phase and water phase in reservoirs with hydraulic conductivity. This pressure difference is then used to locate the free water level (FWL) and the oil-water contact (OWC) can be calculated based on formation properties. Oil and water will have different densities and different pressure gradients. At any point in the reservoir, the difference between these two gradients can be used to calculate the distance down to where the difference is zero, and by definition, the location of FWL.

The OWC is one of the most important parameters for estimating hydrocarbon resources in a reservoir and is usually only known at the start of production. During production, the OWC level is in constant change and its exact position at all times in different parts of the reservoir is unknown. As such, continuous update on the FWL and thus a better estimate of the OWC will have immense value for operators as 1) Planning new wells can be optimized and wells which would quickly yield unwanted water production can be avoided. 2) Knowledge of FWL enables more precise profit analysis of production. Shut-ins can be planned better as water level approaches the well. 3) After a shut-in of a well because of too high water production, continued surveillance can show how the oil column rebuilds over time. Hydrotells tool can thus help increase efficiency, reduce costs, reduce waste and reduce the amount of new production wells. Reduction of produced water will also reduce waste to sea and reduce cost of cleansing and reinjection.

This thesis aim to explore the relation between pressure readings of the tool and the location of the FWL at dynamic conditions using reservoir simulation. This is achieved by building a not overly complicated yet realistic model where mechanisms can be isolated and changed to observe their effect on pressure readings and FWL during production.

Important questions addressed in the thesis are:

- How is the traditional ‘static’ estimate of FWL influenced by a dynamic setting? Is it influenced by how fast production is happening?
- Can water breakthrough be predicted accurately?
- Is the tool reflecting water traveling through a vertical conduit thief zone (or coning) or the more piston-like zone moving upwards?
- Is there a difference in the estimated FWL if the displacement is more or less piston-like?
- How are pressure readings and FWL estimates influenced by parameters such as porosity, compressibility, saturation functions and driving forces?

It starts by showing that the method used in this thesis to locate the FWL only works if a change in capillary pressure takes place, which is dependent on saturation levels at the sensor. As such, if the transition zone is very small, no change in water level is detected until it is almost at the sensor. Next it finds how smaller saturation changes, such as for viscous fingers and thief zones, is not enough to make an impact on the estimate for the FWL. Also, changing capillary curves yielded inconclusive results which could be of interest for further studies. And lastly it finds how receding water yields conflicting results between the estimate of FWL and the actual water level.

Table of Contents

List of Figures

List of Tables

List of Abbreviations

AAPG	American Association of Petroleum Geologists
BHP	Bottom Hole Pressure
DST	Drill Stem Test
FOPT	Field Oil Production Total
FWC	Field Water Cut
FWL	Free Water Level
GWC	Gas Water Contact
NDA	Non-Disclosure Agreement
OPM	Open Porous Media
OWC	Oil Water Contact
RFT	Repeat Formation Test
WBT	Water Breakthrough

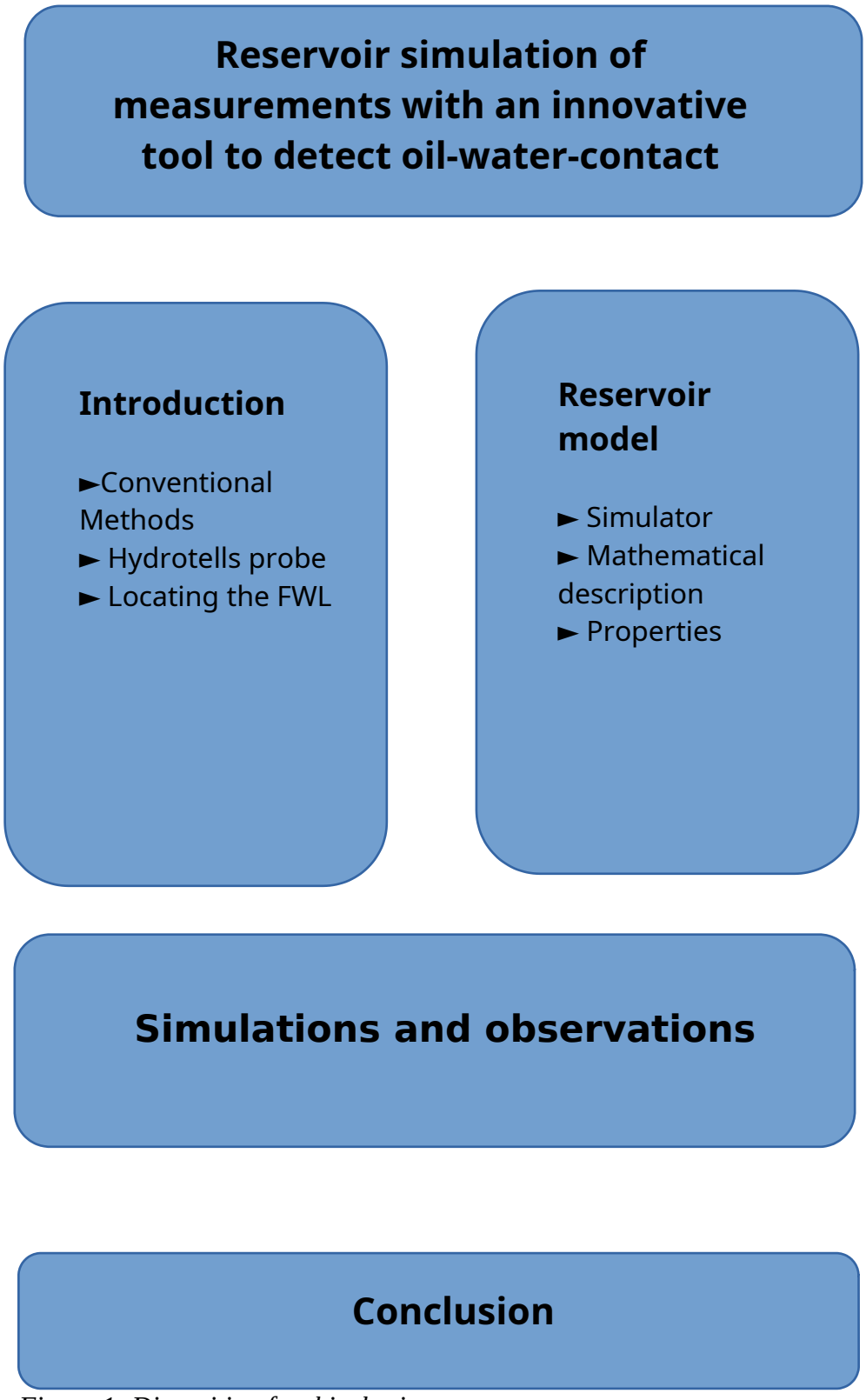

Figure 1: Disposition for this thesis

1 Introduction

The free water level (FWL) in a reservoir is the horizontal plane where water and hydrocarbon pressure are the same. At 100% water saturation there is a minimum capillary pressure needed to force a non-wetting phase into the pore filled with the wetting phase. This minimum pressure is called the displacement pressure p_d (Ahmed, 2010). Oil-water-contact (OWC) is the point above the FWL separated by the displacement pressure. It has been shown that it is possible to measure the pressure of water inside a hydrocarbon reservoir (Rolfsvåg et al., 2019). Their paper describes proof-of-concept tests conducted on core plugs to perform pressure measurements on a thin water film to obtain water pressure independently from the oil pressure inside the core. There they used water- and oil density to predict the pressure differences down the water column based on constructed pressure gradients. However, they also found certain limitations to the concept. If the water phase becomes discontinuous from the aquifer, the water phase pressure will equalize with the oil phase pressure. As such, this method is not suitable for a non-continuous water phase reservoir. Also, the measurement tool can not be too close to the well as mud filtrate can increase the water pressure several meters around the well. If the well was drilled with an oil-based mud, the pore walls will become oil wet and again, the tool must be placed outside of the contaminated zone. They also found that for a precise estimation for the FWL to be possible, the reservoir pressure regime must have come to equilibrium which can be a slow process.

Conventional formation pressure tests are either dependent on having the borehole available for tools (mentioned later) or requires the well to be closed for some time before the test can be done, such as a drawdown test. As such, although 4D seismic logs and history matching simulations based on production can give estimates of current water levels, water pressure can only be measured by stopping production or between drilling which makes such tests a time-consuming and costly affair. Thus, most oilfields are produced without the knowledge of where the FWL is after production has started. FWL or OWC is among the most important parameters in estimating oil reserves of a reservoir. In a producing reservoir the FWL is in constant change, and its position at all times in different parts of the reservoir is unknown. Thus, knowledge of this water level represents a huge potential in cost reduction and efficiency increase in hydrocarbon exploitation.

Hydrotell, a company based in Bergen, Norway, is developing a tool based on the concept mentioned above in order to provide real time measurement of the water pressure in a reservoir, and as an extension, the ability to track the FWL. The concept was shown on a small core plug, and contemporary pressure tests only tests in a static environment. This gives rise to a set of unanswered questions, such as

- The role of thief zones of varying permeability. Is water pressure higher up the column reflecting the thief zone or the piston-like zone moving upwards?
- Is there a difference in the estimates between piston-like displacement and not? That is, will mobile saturations influence pressure reading as fast as the saturation where Pc = 0?
- How is the estimate of FWL influenced by a dynamic setting? Is it influenced by how fast production is happening?
- Which Pc curve yields the best estimate of FWL under dynamic production? Drainage or imbibition?

The goal of this thesis is to create simulations of the pressure differences between oil and water phase in a dynamic situation in hope of determining which mechanisms has the largest impact on pressure readings.

For this task, for the sake of convenience and licensing limitations, the open source Eclipse-like program Open Porous Media (OPM) Flow was selected as the simulator, and the program ResInsight was selected for the data presentation and reservoir visualization.
Simulations include changes in capillary pressure curves, oil viscosity, permeability for specific zones, production rate and shut-in of the well. It was found that saturation levels plays an important role in the estimation for the free water level. Unless there is a change in water saturation, the capillary pressure seems to be unchanged in all scenarios, leaving the distance to FWL in a constant position. This means that if the sensor is placed in a place above the transition zone, the method used in this thesis can not be used reliably. As such, we observed how a higher transition zone led to a shorter distance to FWL, although these simulations also produced some inconclusive results. Moreover, it was shown how columns of water, such as thief zones or viscous fingers would not be detected which meant the FWL further down in the reservoir would be correctly estimated as further down, while the water breakthrough would not be seen in advance.
However, we also saw how the positioning of the thief zones made no difference to the estimate of the FWL, meaning the distance would be correctly estimated even if the FWL is not directly beneath the sensor. Lastly it was found that receding water seemingly gave conflicting results where the estimate showed an increase in distance while what actually happened was a decrease in distance.

As the scope of this thesis can quickly become vast, certain limitations had to be put in place. Real-life testing on cores has been done earlier, and thus not conducted for this thesis. Limitations of the chosen simulator led to removal of capillary pressure hysteresis and Leverett J-scaling. Horizontal thief zones, varying permeability layers, multiple producers over a field, chemical injections and related effects, bacterial flora and a system containing gas, are all valid scenarios that could be looked into but has been reserved for future work.

1.1 Conventional Methods

Niculescu and Ciuperca (2019) describes how fluid contacts can vary over a reservoir either because of faults, semipermeable barriers, rock quality variations or reservoir heterogeneity, hydrocarbon drainage/imbibition history or hydrodynamic activity. They further mentions several methods for determining fluid contacts such as fluid sampling, saturation estimates from geophysical well logs, core analysis and formation pressure measurements and points out that the latter is the primary source of data for defining the fluid contacts.

According to the American Association of Petroleum Geologist (AAPG) wiki page, the most common fluid pressure measurements in use (AAPG, 2022c) are

- Drill stem test (DST) shut-in pressures
- Repeat formation test (RFT)
- Reservoir bottom-hole pressure buildup tests

They will be mentioned briefly and not discussed at length.

1.1.1 DST shut-in pressures

As Dolan et al. said (1957), "a drill-stem test is a temporary completion designed to sample the formation fluid and to establish the possibility of commercial production". In this test, packers are placed around an empty drill pipe, allowing formation fluid flow into the pipe. The open-hole DST gives a variety of information: permeability, flow rates, skin damage and water production (Hoyer et al., 1996). Open-hole means that if bottom hole pressure (BHP) is sufficient, fluid will be produced at the surface. However, a typical DST will have a shut-in period where the tools valve is closed and pressure will ideally build up in the tool until it reaches equilibrium with the pressure of the isolated formation. However, accurate pressure is difficult to obtain for DST in low-permeability zones such as chalk. Moreover, this pressure may not be reliable because the tool is not shut in long enough for pressure to stabilize. Packer failure and depth determination are also sources of survey failure (AAPG, 2022b).

1.1.2 Repeat Formation Test

The RFT, earlier called "sequential formation testing" (Soliman et al., 1988), measures pressure at several points down the borehole. This lets the user plot a graph of points to construct pressure gradients. OWC and GOC can then be found by finding the crossover points by the different gradients (AAPG, 2022a). The ability to test multiple zones and take fluid samples from them in a rapid manner, is a major limitation to the DST (Hoyer et al., 1996), which is adressed by the RFT by design. However, screen plugging with material in drilling mud and getting a good seat to measure pressure are challenges facing the RFT.

1.1.3 Pressure buildup test and Drawdown test

A pressure buildup test is similar to the DST shut-in pressure, however in this case the well is already a producing well. This means the well is shut in at the surface to let the bottom hole pressure build up. This lets the operator read a variety of information such as bottom hole pressure, well flow capacity, permeability thickness, skin effect and other information (Schlumberger, 2022). Similariliy, pressure drawdown tests are a series of pressure measurements that can be run after production has started in order to measure the formation pressure. Again the well is shut in for some time ahead of the test to allow the pressure to become equal throughout the formation. It is shut in until it reaches a constant reservoir pressure. The well is then opened and produced at a constant flow rate, while continuously recording bottom-hole pressure. When a constant flow rate is attained, the pressure measuring equipment is lowered into the well. It may take a few hours to several days, depending on the objectives of the test (Khan & Islam, 2007).

The above mentioned tests all measure the formation fluid pressure, that is, the hydrocarbon pressure. All tests can locate the FWL if the well intersects the FWL as shown in figure 2a. Formation pressure is measured at different depths and FWL will be located where the pressure curve shifts as shown in figure 2b. Thus, the OWC can be estimated based on the determined depth of the FWL. However, several types of traps and several combinations of them can make one single discovery well insufficient (Capotosto et al., 2021). Common for all three tests is that drilling or production is delayed. Moreover, in order to see transient development of pressures, production must be stopped several times over time, which usually leads to such tests being scarce after startup.

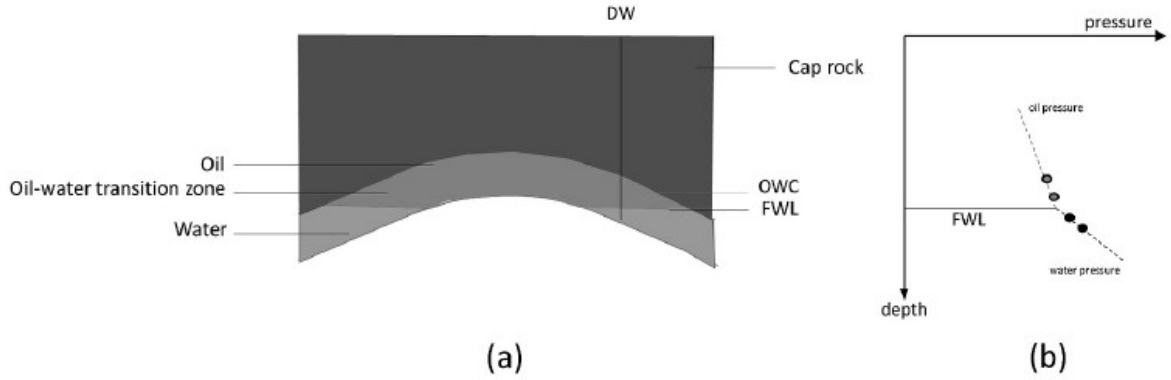

Figure 2: a) A well drilled through a typical fluid distribution in a convex trap. b) How conventional pressure tests locates FWL (Capotosto et al., 2021).

1.2 Hydrotells probe

The probe in development by Hydrotell is based on a technology developed by Hydrophilic. Different from Hydrophilic, however, Hydrotells probe is meant to be permanently installed into production wells where it can monitor the water phase pressure in producing fields without stopping production and thus continuously locate the FWL.

The probes tip is designed such that water can move through, but not oil. This means the water phase pressure inside the oil column can then be measured separately. Water pressure can be found with conventional pressure tests, if gradients are constructed from tests at different depths as shown above. However, measuring the water phase pressure inside the hydrocarbon phase is unique to Hydrotells technology, and in conjunction with tests such as the drawdown test, both oil and water phase pressure at a single depth will be known factors.

Thus, together with the known phase densities, the information can then be used to estimate the distance down to FWL.

Continuous update on the FWL and thus a better estimate of the OWC will have immense value for operators as

1. Planning new wells can be optimized and wells which would quickly yield unwanted water production can be avoided.
2. Knowledge of FWL enables more precise profit analysis of production. Shut-ins can be planned better as water level approaches the well.
3. After a shut-in of a well because of too high water production, continued surveillance can show how the oil column rebuilds over time. Hydrotells tool can thus help increase efficiency, reduce costs, reduce waste and reduce the amount of exploration wells. Reduction of produced water will also reduce waste to sea and reduce cost of cleansing and reinjection.

1.3 Locating the free water level

Capillary forces in a petroleum reservoir are the result of the combined effect of surface and interfacial tensions of the rock and fluids, the pore size and geometry and the wetting of the system. When two immiscible fluids are in contact, a discontinuity in pressure exists between the two fluids, which depends upon the curvature of the interface separating the fluids (Ahmed, 2019). This pressure difference between non-wetting and wetting phase is called the capillary pressure, p_c, and is defined by Lake (1989) as

$$p_2 - p_1 = \frac{2\sigma \cos\theta}{R} \equiv p_c \tag{1}$$

Equation (1) relates the capillary pressure across an interface to the curvature of the interface R, the interfacial tension σ and the contact angle θ. The equation shows that the capillary pressure can only be zero if the interfacial tension is zero or the interface is perpendicular to the tube wall which only holds true in simple uniform tube geometry and is not relevant in a reservoir. As such, this thesis use the definition of capillary pressure as only the pressure difference between non-wetting phase and wetting phase, that is oil and water respectively. Thus

$$p_c = p_{oil} - p_{water} \tag{2}$$

The FWL is defined as the depth where the oil pressure is equal to the water pressure making the capillary pressure equal to zero (Ahmed, 2010). The oil-water contact is immediately above the FWL and it is defined as the lowest depth at which mobile oil occurs (Elshahawi, Fathy, and Hiekal 1999), shown in figure 3.

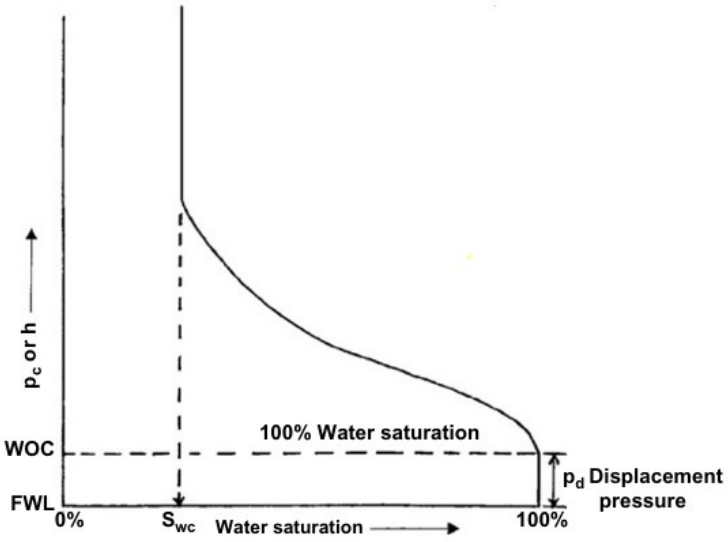

Figure 3: Capillary pressure curve denoting zero capillary pressure at free water level and displacement pressure separating OWC and FWL (Ahmed, 2019).

To locate FWL, this thesis will use the technique described by Rolfsvåg et al. (2019), shown in figure 4 where the water pressure is measured inside the oil reservoir and by knowing the densities of the water and the oil, the pressure trends can be extrapolated downwards. The FWL is where the lines cross.

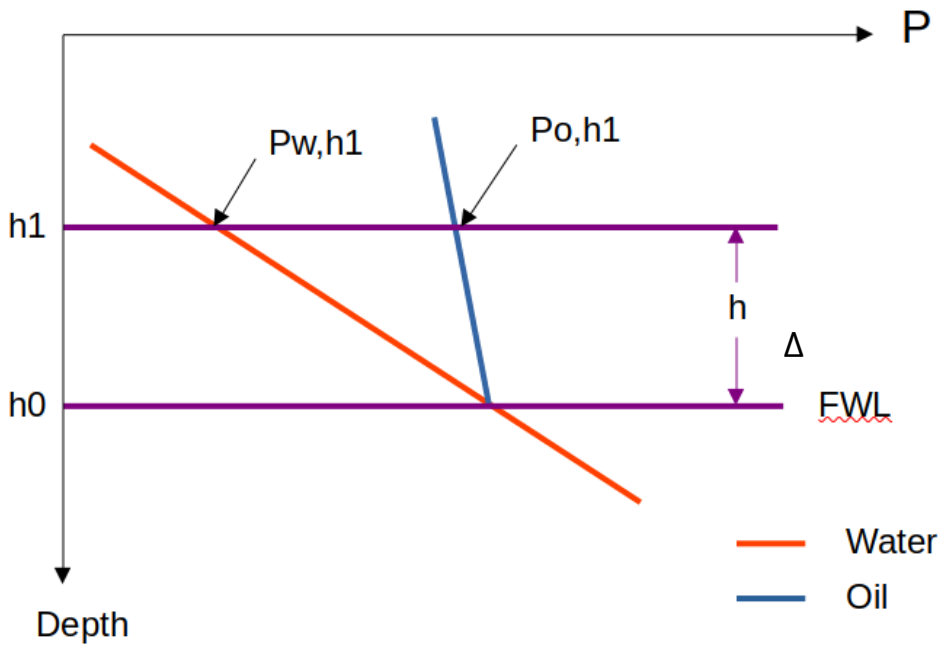

Figure 4: Method for locating FWL at h0. Pressure difference is measured at h1 some depth Δh above h0.

The pressure graphs and their corresponding convergence point at h_0 in figure 4 is constructed like this:

With measured points at h_1, an arbitrary depth h_j between h_1 and h_0 would have a capillary pressure of

$$p_{cj} = (p_{o,h_1} + \rho_o g \Delta h_j) - (p_{w,h_1} + \rho_w g \Delta h_j) \quad (3)$$

where $p_{i,h1}$ is measured pressure of phase i (i = o, w) at depth h_1, ρ_i is phase density in [kg/m³], g is gravity constant in [kg*m/s²] and Δh_j is change in depth from measuring depth down to h_j.

Hydrotells tool will measure all three pressures in equation (2) and as mentioned above, FWL is defined as the depth where $p_c = 0$. Thus, locating FWL is now the simple task of setting equation (3) equal to zero and solve for Δh to obtain

$$p_{c,0} = 0 = p_{o,h_1} + \rho_o g \Delta h - p_{w,h_1} - \rho_w g \Delta h$$

$$\Delta h = \frac{p_{c,h1}}{g(\rho_w - \rho_o)} \quad (4)$$

Thus, Δh represents the distance from measured pressure difference down to FWL.

As seen in figure 3, FWL is generally not coincident with OWC but differs by an amount related to the displacement pressure, p_d. In a water-wet reservoir FWL will occur at some depth d below OWC given by (Elshahawi et al., 1999):

$$d = \frac{p_d}{\rho g} \tag{5}$$

where p_d is the displacement pressure of oil displacing water in [Pa].

2 Reservoir Model

2.1 The simulator

For this project, the Open Porous Media (OPM) Flow simulator was chosen. OPM Flow is an open source alternative to industry standards, which means all software and data sets are available for use by anyone. OPM Flow "*aims to represent reservoir geology, fluid behavior, and description of wells and production facilities as in commercial simulators and hence offers standard fully-implicit discretizations of black-oil type models and supports industry-standard input and output formats*." (Rasmussen et al., 2021). OPM Flow is using the black-oil model which is based on the premise that there are three different fluid phases (aqueous, oleic and gaseous) and three components (water, oil and gas). Oil and gas can be found in oleic phase, in the gaseous phase or in both. However, for this project, gas has been omitted, leaving only water and oil, which are immiscible.

2.2 Mathematical description

The black-oil equations can be deducted from conservation of mass for each component with suitable closure relationships such as Darcy's law and initial boundary conditions. In OPM Flow they are "*discretized in space with an upwind finite-volume scheme using a two-point flux approximation and in time using an implicit (backward) Euler scheme. The resulting equations are solved simultaneously in a fully implicit formulation by a Newton-type linearization with a properly preconditioned, iterative linear solver*" (Rasmussen et al., 2021).

Equations presented here assume flow of two immiscible and compressible fluids, oil (o) and water (w) in a 3-dimensional space.

In compact form, for oil and water phase

$\boldsymbol{\nu_i} = (\nu_{ix}, \nu_{iy}, \nu_{iz}),\ (i = o, w)$ is the Darcy velocity vector in [m/s], given by

$$\boldsymbol{\nu_i} = -\frac{\boldsymbol{K}\, k_{ri}}{\mu_i}(\nabla p_i - \rho_i g \nabla z),\ (i = o, w) \tag{6}$$

Where **K** is the absolute permeability (k_x, k_y and k_z), $\boldsymbol{\nu_i}$ is Darcy velocity vector, k_{ri} is relative permeability, μ_i is viscosity, p_i is pressure, g is the acceleration of gravity (9.81 m/s^2), and z is depth. The subscript i denotes phase.

As the two components are immiscible, they are only stored and transported in their own phase. Thus, by adding a source term q to the continuity equation, mass balance is described by

$$\nabla \cdot (\rho_i \boldsymbol{\nu_i}) = -\partial_t(\phi \rho_i s_i) + q_i\ ,\ (i = o, w) \tag{7}$$

Where Φ is porosity and ρ_i is phase density and s_i is saturation.

The four variables s_o, p_o, s_w and p_w are constrained by volume conservation and capillary pressure,

$$S_o + S_w = 1,\ P_{cow}(S_w) = p_o - p_w \tag{8}$$

If the mobility ratio

$$\lambda_i = \frac{k_{ri}}{\mu_i},\ \lambda_T = \lambda_o + \lambda_w \tag{9}$$

Then the total Darcy flux vector $\mathbf{v}_T$ is then defined by using equation (6)

$$\begin{aligned} \boldsymbol{\nu_t} &= \boldsymbol{\nu_o} + \boldsymbol{\nu_w} = -\boldsymbol{K}\lambda_o(\nabla p_o - \rho_o g \nabla z) - \boldsymbol{K}\lambda_w(\nabla p_w - \rho_w g \nabla z) \\ &= -\boldsymbol{K}(\lambda_o \nabla p_o - \lambda_o \rho_o g \nabla z + \lambda_w \nabla p_w - \lambda_w \rho_w g \nabla z) \end{aligned} \tag{10}$$

Substituting ∇p_o *for* $\nabla p_c + \nabla p_w$ yields

$$\boldsymbol{\nu_t} = -\boldsymbol{K}(\lambda_o(\nabla p_c + \nabla p_w) - \lambda_o \rho_o g \nabla z + \lambda_w \nabla p_w - \lambda_w \rho_w g \nabla z) \tag{11}$$

which is then rewritten as

$$\boldsymbol{\nu_t} = -\boldsymbol{K}\lambda_T \nabla p_w - \boldsymbol{K}\lambda_o \nabla p_c + \boldsymbol{K}(\lambda_o \rho_o + \lambda_w \rho_w) g \nabla z \tag{12}$$

and λ_i and λ_T is the phase and total mobilities, respectively. Equation (12) can be solved for ∇p_w

$$\nabla p_w = \frac{\boldsymbol{\nu_t} + \boldsymbol{K}\lambda_o \nabla p_c - \boldsymbol{K}(\lambda_o \rho_o + \lambda_w \rho_w) g \nabla z}{-\boldsymbol{K}\lambda_T} \tag{13}$$

Then, if f_i is the fractional flow function of phase i.

$$f_i = \frac{\lambda_i}{\lambda_T},\ (i = o, w) \tag{14}$$

it can be substituted to produce the following

$$\nabla p_w = -\frac{\boldsymbol{\nu_t}}{\boldsymbol{K}\lambda_T} - f_o \nabla p_c + f_o \rho_o g \nabla z + f_w \rho_w g \nabla z \tag{15}$$

Then, for the water phase, putting equation (6) into (7) gives

$$\partial_t(\phi \rho_w s_w) - q_w = -\nabla \cdot (\rho_w [-\boldsymbol{K}\lambda_w(\nabla p_w - \rho_w g \nabla z)]) \tag{16}$$

Now, substituting ∇p_w with equation (15) gives

$$\partial_t(\phi \rho_w s_w) - q_w = -\nabla \cdot (\rho_w [-\boldsymbol{K}\lambda_w(\frac{-\boldsymbol{\nu_t}}{\boldsymbol{K}\lambda_T} - f_o \nabla p_c + f_o \rho_o g \nabla z + f_w \rho_w g \nabla z - \rho_w g \nabla z)])$$

$$\begin{aligned} \partial_t(\phi \rho_w s_w) - q_w &= \nabla \cdot (-\rho_w f_w \boldsymbol{\nu_t}) - \nabla \cdot (\rho_w \boldsymbol{K}\lambda_w f_o \nabla p_c) + \\ &\quad \nabla \cdot (\rho_w \boldsymbol{K}\lambda_w g \nabla z [f_o \rho_o + f_w \rho_w - \rho_w]) \end{aligned} \tag{17}$$

If we say that the total flow is unity, and comprise two fractions, then

$$f_w + f_o = 1 \rightarrow -f_o = f_w - 1$$

$$\partial_t(\phi \rho_w s_w) - q_w = \nabla \cdot (-\rho_w f_w \boldsymbol{\nu_t}) - \nabla \cdot (\rho_w \boldsymbol{K} \lambda_w f_o \nabla p_c) + \nabla \cdot (\rho_w \boldsymbol{K} \lambda_w g \nabla z [f_o \rho_o + (f_w - 1)\rho_w]) \quad (18)$$

$$\partial_t(\phi \rho_w s_w) - q_w = \nabla \cdot (-\rho_w f_w \boldsymbol{\nu_t}) - \nabla \cdot (\rho_w \boldsymbol{K} \lambda_w f_o \nabla p_c) + \nabla \cdot (\rho_w \boldsymbol{K} \lambda_w g \nabla z f_o [\rho_o - \rho_w]) \quad (19)$$

Where ρ_i is phase density, q_w is source term (rate), f_i is the fractional flow, **K** is the absolute permeability, $\boldsymbol{\nu_i}$ is Darcy velocity vector, λ_i is mobility ratio, z is depth, φ is porosity, g is gravity constant, s_w is water saturation and p_c is capillary pressure.

For more in-depth mathematical description of the simulator, please refer to the works of (Andersen, 2021) and (Nygård & Andersen, 2020).

2.3 Size, shape and content

The model is a modification of SPE1_Case2 which is available from the OPM homepage. It was used as a basis for this project as it contained a run with only black oil and water.

The model was expanded to 2x2 km across and 200m deep. This larger size meant there was enough oil content so that the FWL would hardly rise after 5 years of production. This defeated our purpose and it was later changed to a 1x1 km across and 200m deep reservoir.

The final size and shape is given in table 1 and as can be seen in figure 5, a horizontal well was chosen for this model. This was done first and foremost because vertical wells are hardly in use today but also because a horizontal well

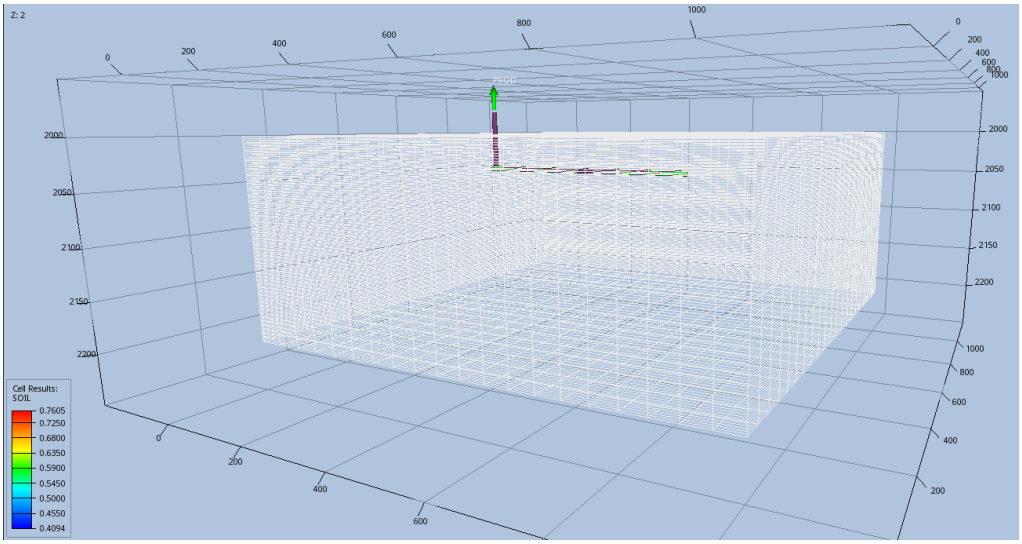

Figure 5: Final shape of reservoir model

could spread the oil drainage over a larger area without the need for several vertical wells. Here it should be noted that in OPM, a string of vertical wells in blocks next to eachother is interpreted as a horizontal well. A horizontal well is then also chosen out of simplicity.

The input deck for the model can be found in the appendix.

Table 1: Reservoir size and shape for OPM model

Direction	Size	Grid	Aquifer	Wells (gridblocks)	Injectors
X	1 km	20	Fetkovich	5 – 15	None
Y	1 km	20		10	None
Z	200 m	100	150 – 200 m	20	None

2.3.1 Choice of aquifer

In almost all cases of reservoirs, they will be surrounded by water-bearing rocks called aquifers. These can range from so large in size they can seem infinite to so small that they are negligible in their effect on reservoir performance. As pressure declines in the reservoir during production, a pressure differential develops from the surrounding aquifer into the reservoir. In some cases the pore volume of the aquifer is the same as the reservoir or not significantly larger. If so, the expansion of the water in the aquifer is negligible relative to the overall energy system and the reservoir behaves volumetrically. In that case, the effects of water influx can be ignored. Another case is if the aquifer has a relatively low permeability. In that case, a large pressure differential must build up before a meaningful water influx is attained (Ahmed & McKinney, 2005). The purpose here is to have a large enough aquifer with high enough permeability to provide a steady influx of water as pressure drops in the reservoir. The same could be achieved using multiple water injectors, but an aquifer will provide a more even distribution of water across the OWC. Thus, its main purpose in this model is to act as an active water drive for oil production, that is, “the water enroachment mechanism in which the rate of water influx equals the reservoir total production rate” (Ahmed & McKinney, 2005).

Two aquifers are available in OPM Flow: Fetkovich and Carter-Tracy. The model in this thesis uses the Fetkovich aquifer which has an influx of water proportional to pressure drop in the aquifer.

Fetkovich described the aquifer in detail in (1971) and is based on the premise that the productivity index concept will adequately describe water influx. The Fetkovich method starts with two basic equations, the productivity index equation:

$$e_w = \frac{dWe}{dt} = J(\bar{p_a} - p_r) \tag{20}$$

and the material balance equation for a constant compressibility (equation 22).

However, the model has evolved over time and contemporary simulators such as Flow and Eclipse use an aquifer inflow model based on the equation (Schlumberger, 2014):

$$Q_{ai} = \frac{d}{dt}(W_{ai}) = J\,\alpha_i[p_a + p_c - p_i + \rho g(d_i - d_a)] \tag{21}$$

where Q_{ai} is the inflow rate from aquifer to connecting grid block i, W_{ai} is the cumulative influx from the aquifer to grid block i, J is a productivity index specified in the simulator, α_i is the area fraction for the connection to grid block i, p_a is the pressure in the aquifer at time t, p_c is the capillary pressure, p_i is the water pressure in a connecting grid block I, ρ is water density in the aquifer, d_i is the depth of grid block i, d_a is the datum depth where the aquifer is connected to the reservoir.

The pressure response in the aquifer which states that the amount of pressure depletion in the aquifer is directly proportional to the amount of water influx from the aquifer (Ahmed & McKinney, 2005) is also described by (Schlumberger, 2014):

$$W_a = C_t V_{w0}(p_{a0} - p_a) \tag{22}$$

where W_a is the cumulative total influx from the aquifer, C_t is total compressibility (rock + water), V_{w0} is initial volume of water in the aquifer and p_{a0} is initial pressure of water in the aquifer. W_a is incremented at the end of each timestep and its pressure is updated using equation (22)

When the p_{a0} value is defaulted in OPM Flow, the simulator will set the initial pressure to be in equilibrium with the connecting grid blocks. With the assumption of this pressure being uniform and by integrating equation (21) and (22) we obtain the equation for average influx from the aquifer used by the simulators:

$$\bar{Q}_{ai} = \alpha_i J(p_a - p_i + \rho g(d_i - d_a))\left(\frac{1 - e^{(-\Delta t / T_c)}}{\Delta t / T_c}\right) \tag{23}$$

where $\bar{Q}_{ai}$ is the average influx of water into the reservoir, T_c is the aquifer time constant and is given by

$$T_c = \frac{C_t V_{w0}}{J} \tag{24}$$

We see from equation (23) and (24) that if $C_t V_{w0}$ (and by extension, T_c) is allowed to be big, i.e. large volume of initial water, then the time constant is large enough to make the last part of equation (23) approach 1. This results in the boundary pressures remaining unchanged and the aquifer takes on a steady-state behavior. However, if say J is allowed to be large, T_c becomes small and the pressure will be in approximate equilibrium with the reservoir at all times.

2.4 Leverett J-scaling (JFUNC)

The capillary pressure at a given saturation is a measure of the smallest pore being entered by the non-wetting phase at that point, suggesting the curvature of the capillary pressure curve is a function of pore size distribution (Lake, 1989). Additionally, capillary pressure data are measured on core plugs with varying quality and perhaps from different reservoirs. It is therefore necessary to determine averaged data, before employing the data in engineering calculations. Leverett (1941) proposed how this could be done with a non-dimensional form of the drainage capillary pressure curve that should be independent of the pore size. The Leverett J-function, is defined by the OPM reference manual (Baxendale, 2021) as

$$J(S_w) = \frac{P_{c,res}(S_w)\left(\frac{k^{\beta}}{\varphi^{\alpha}}\right)}{\sigma}$$

where *J (Sw)* is a dimensionless function of water saturation. J depend only on saturation and is the same everywhere . *Pc,res* is the capillary pressure at reservoir conditions, *k* is permeability, φ is porosity and σ is interfacial tension. The power values α and β can be scaled in the model, however in this thesis they are kept at the standard 0.5, thus the equation takes the following form:

$$J(S_w) = \frac{p_{c,res}(S_w)\sqrt{\frac{k}{\varphi}}}{\sigma} \tag{25}$$

Equation (25) is actually a combination of equation (1) and a single-phase, one-dimensional permeability equation given by Lake (1989) as

$$k = \frac{R^2 \varphi}{8\tau} \tag{26}$$

where R is radius, φ is porosity. The tortuosity τ and the numerical constant has been absorbed by J in equation (25).

It should here be noted that after substantial trial and error, it was discovered that the J-function values entered in the input deck was not read correctly or not calculated correctly by OPM Flow, and lead to erroneous capillary pressure curves and any estimates involving capillary pressure would produce incorrect results. As the data used from Kleppe and Morse (1974) were scaled with the J-function, it was decided to reverse formula (25) in Excel to find the Pc curves instead of the J-curves, and then use these values in the input deck.

2.5 Hysteresis

A reservoir will most likely be filled with water before oil enters the reservoir and reduces the water content down to a certain residual water saturation. As such, any found hydrocarbon reservoir starts with a certain connate water saturation (unmovable water). The process of generating the capillary pressure curve by displacing the wetting phase i.e. water, with the nonwetting phase (such as gas or oil), is called the drainage process. Equally, when the non-wetting phase is displaced by the wetting-phase, the process is reversed, but the curve will not take the same path. The resulting curve is called the capillary pressure imbibition curve (Ahmed, 2010). Thus different curves will be generated over time as imbibition and drainage takes place.

This concept is also true for relative permeabilities. At some low saturation, hydraulic conductivity is lost and flow stops. This saturation is often referred to as the residual saturation. Also, the fluid must reach a certain saturation in order to begin flow. This is referred to as the critical saturation. These two saturations are not equal as the "*critical saturation is measured in the direction of increasing saturation, while irreducible saturation is measured in the direction of reducing saturation. Thus the saturation histories of the two measurements are different*" (Ahmed, 2010). As such, as discussed for capillary pressure data, there is a history effect for relative permeability as shown in figure 6. The difference in relative permeability and/or capillary pressure when changing the saturation history is called hysteresis. For the sake of this models water phase pressure measurements, capillary pressure hysteresis was a wanted option. However, it was discovered that OPM Flow (as of version 2022.04) only support the relative permeability data in implementing hysteresis. Thus, capillary pressure hysteresis was unavailable. It was then decided that hysteresis would be taken out of the model as it could lead to unwanted or "harder-to-interpret"-results.

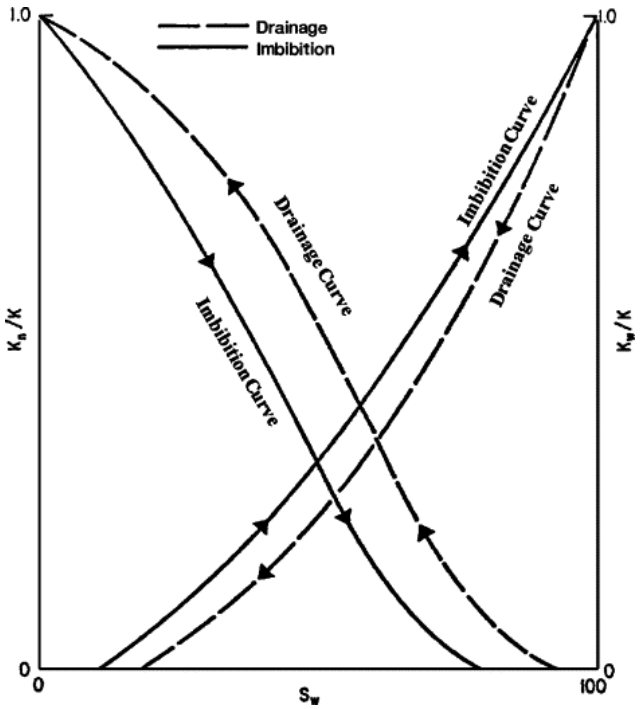

Figure 6: Hysteresis effects in relative permeability (Ahmed, 2010).

2.6 Properties

Table 2: Base reservoir properties for the OPM Flow reference model

Permeability	X = 256 mD	Y = 256 mD	Z = 256 mD
Saturation	Swr = 0.3	Sor = 0.395	
Porosity	0.218 for all cells		
Rock Type	Berea Sandstone		
Fractures	None		
Water	Compressibility = 4.67E-5 [1/bar]	Viscosity = 0.87 [cp]	Viscosibility = 0 [1/bar]
Liquid prod. rate	3000 [sm³/d]		
Production well	Xloc= 5-15	Yloc = 10	Zloc = 20

Several key input data used in the reference model is shown in table 2. For the saturation, relative permeability and J scaling curves, several data sets were tried before the author became aware of J-scaling not working correctly in OPM Flow. The data set were systematically tested in the simulator without yielding realistic results (such as a non-existent transition zone). Some data were supplied by Arild Lohne at Norce, but in the end, data from Kleppe and Morse (1974) were used and scaled with an extended corey formula provided by Pål Ø. Andersen. However, even with the scaling, krw would surpass 1, as seen in figure 7, and could not be used.

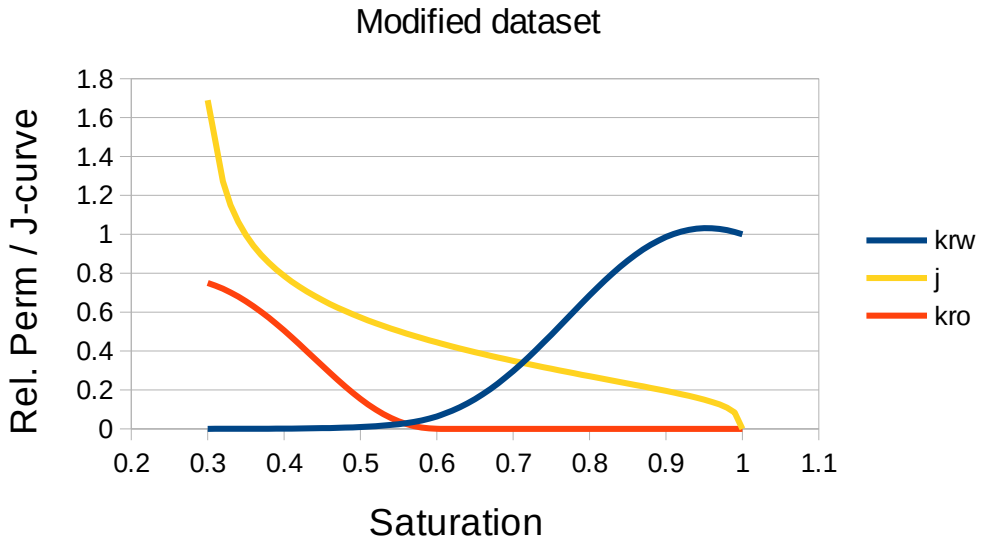

Figure 7: Kleppe and Morse data scaled with extended corey formula. Krw curve surpass 1 and could not be used. J function curve which was later discarded is in yellow.

Thus, a “quick” solution was to create a linear line for krw between saturations 1-Sor (0.605) and 1. This would ensure an intact crossing of the curves, and provide a steady increase in krw up to a saturation of 1. Also, after the J-function had been reversed, the highest Pc value at Sw = 0.3 was only 0.7. This resulted in a very small transition zone and meant that Pc would not change until the top of this zone would reach the sensor at the well. This in turn meant that the calculation for FWL would remain constant until a change in saturation levels occurred as we will see is still the case later. The final dataset used in the reference model can be seen in figure 8.

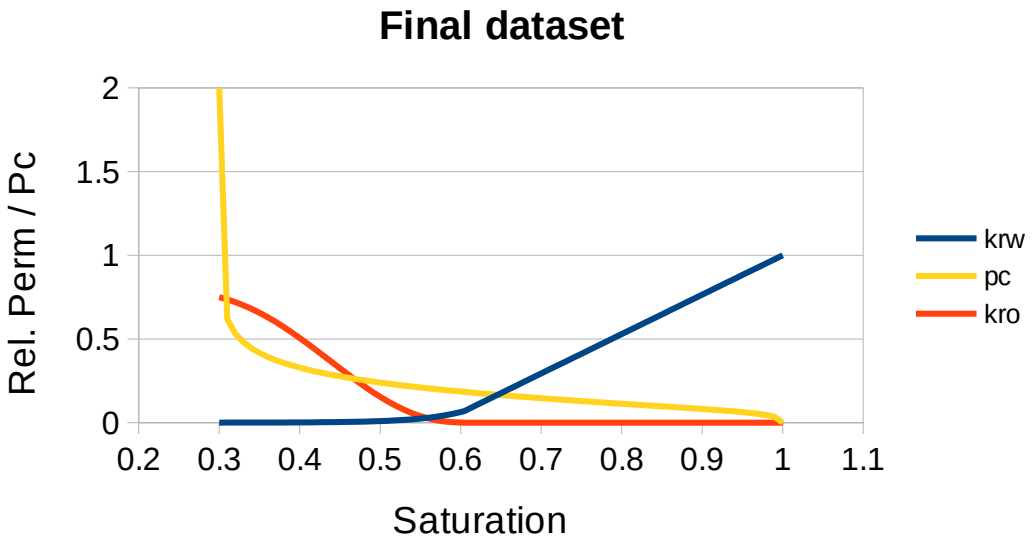

Figure 8: Final saturation curves used in the reference model. Reverse calculated Pc curve in yellow.

3 Results

3.1 Reference model

First, as seen in figure 9, field water cut remain at zero until 2025-01, meaning we have water breakthrough (WBT) after about 3 years. Thus, this timestamp is a point of interest. An uneven increase in water cut takes place for about six months before we see a steady increase in water cut until end of production, ending after 5 years with a produced water fraction around 15%.

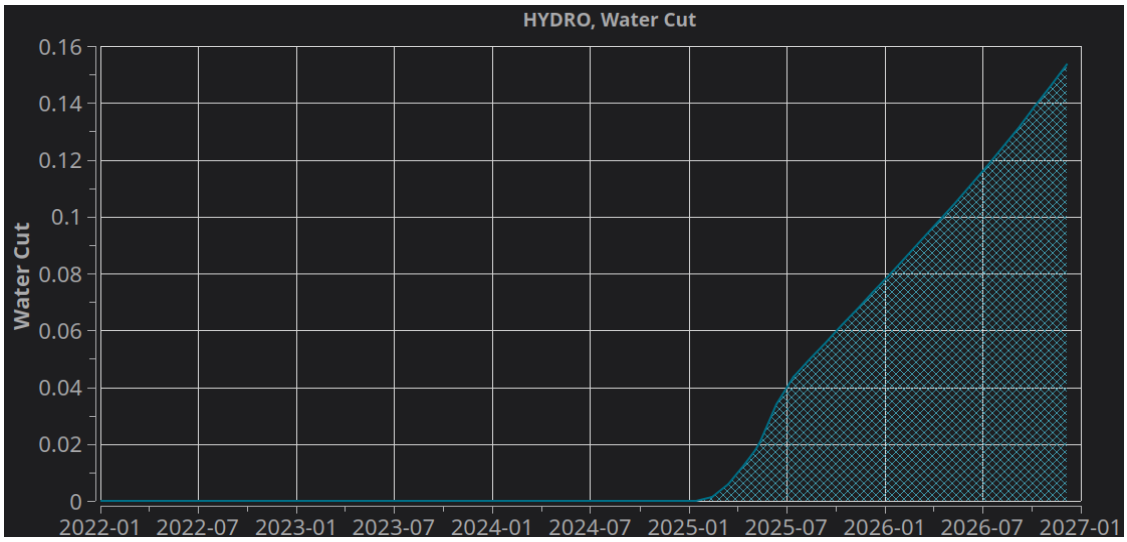

Figure 9: Field water cut for reference model. Water breakthrough happens after three years of production.

The water phase pressure shown in figure 10 is measured in block (11,11,20). This block is at the same depth as the horizontal well and is one of the connecting blocks.

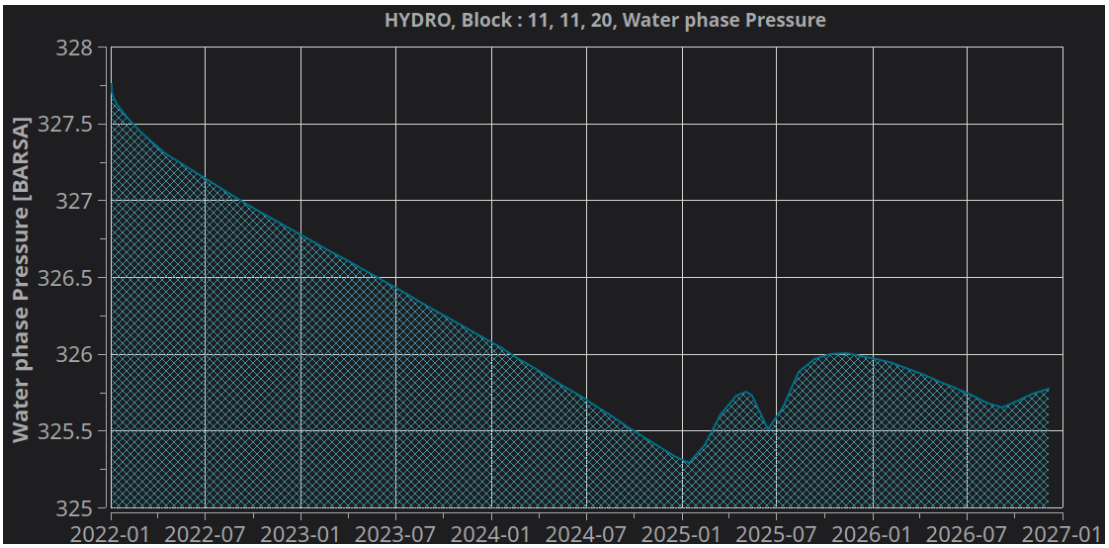

Figure 10: Water phase pressure for block (11,11,20) next to the producing well.

As we know that Hydrotells measurement tool can not be installed inside the well, this block was chosen as it is the best representative to a possible location although it must be mentioned

that the blocks in horizontal directions are 50m across, and Hydrotells unit would not be installed 50m away from the well.

However, it is still a well-connecting block and should represent what could be observed in a real reservoir. Thus, further measurements of other cases will also be measured in this block. As seen in figure 10, the water phase pressure steadily decreases from start of run until WBT. At WBT a very uneven behaviour is observed until end of production, starting with a quick increase for the next 4 months, then rapid decrease for the next two. After WBT, a peak of 326 bar is observed at November 2025, almost a year after WBT.

We may now implement equation (4) in ResInsight to see how the FWL is rising based on the formula. As FWL rises during production, Δh should decrease steadily until WBT. However, what is observed in figure 11 is that the FWL is at an almost constant 88 m down the reservoir until WBT which was established above at 2025-01.

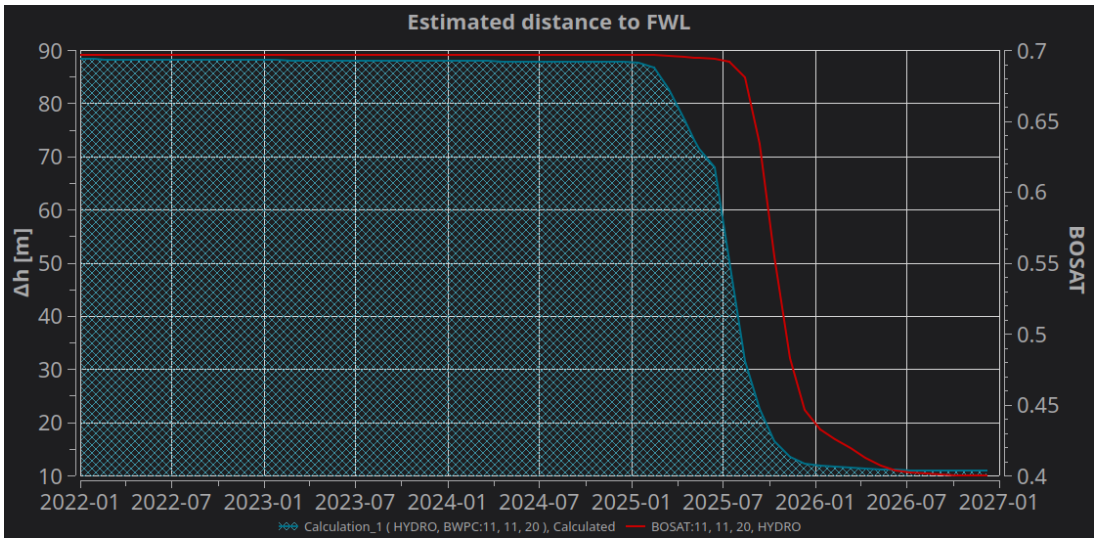

Figure 11: Esimated distance to FWL from block (11,11,20). Oil saturation is shown in red. It is observed that only slight saturation changes happen before WBT.

When FWL starts to decrease, it decreases rapidly over a course of about 8 months before it flattens out at about 11m, signaling that FWL should be at a constant 11m depth from the well. The reason for this is that Pc must become zero for equation (4) to become zero. This will not happen as Pc(1-Sor) > 0. Pc is only zero at the bottom of the transition zone. A shift in the Δh curve is observed right before the 2025-07 mark, which corresponds to a bottom of a dip in the water phase pressure. Comparing figure 10 and 11, we see a steady decrease in the water phase pressure while Δh remain unchanged indicating that water phase and oil phase pressure both decline steadily, keeping Pc unchanged.

What is also observed from figure 11 is the relationship between oil saturation (in red) and the estimated distance. The FWL starts to increase at the same time as oil saturation starts to decrease. Again this makes sense as Pc is a function of the water saturation. Thus, Pc is unchanged as long as saturation levels remain unchanged. Only negligible saturation changes is observed for the first three years, and consequently Δh seem almost constant for this period.

It should be noted that if hysteresis had been implemented as intended, these graphs would turn out differently. In that case, Δh would eventually become zero given enough time.

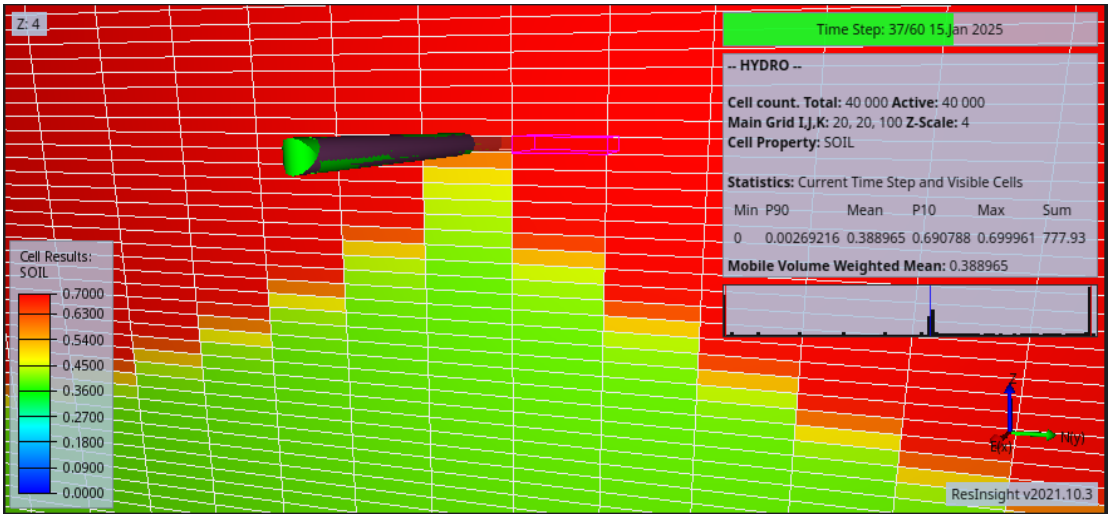

Figure 12: Cross section view through the x-axis showing oil saturation levels at WBT showing WBT has yet to happen for block (11,11,20)

An I-slice (a cross section through the x axis) which shows the saturation states at the time of WBT for cells (11,5-15,10-46) can be seen in figure 12. Here it is observed that WBT has yet to happen for the marked block (11,11,20). Also, each block in z-direction is 2m thick. This means the water front can be seen at 12m down the column.

If we define the “real” FWL as “the point where water saturation has reached 1-Sor”, then FWL is indeed much deeper in the reservoir. In fact, figure 13 shows a water saturation of 0.605 was not observed until block z=65, corresponding to 65-20 = 45 blocks → 45*2m = 90m. 90m fits the observed results in figure 11 of an FWL estimate of 88m. However, this was only at WBT. At earlier times, such as 2022-02, such high water saturation is not reached until block 69, which would mean a Δh of 98m.

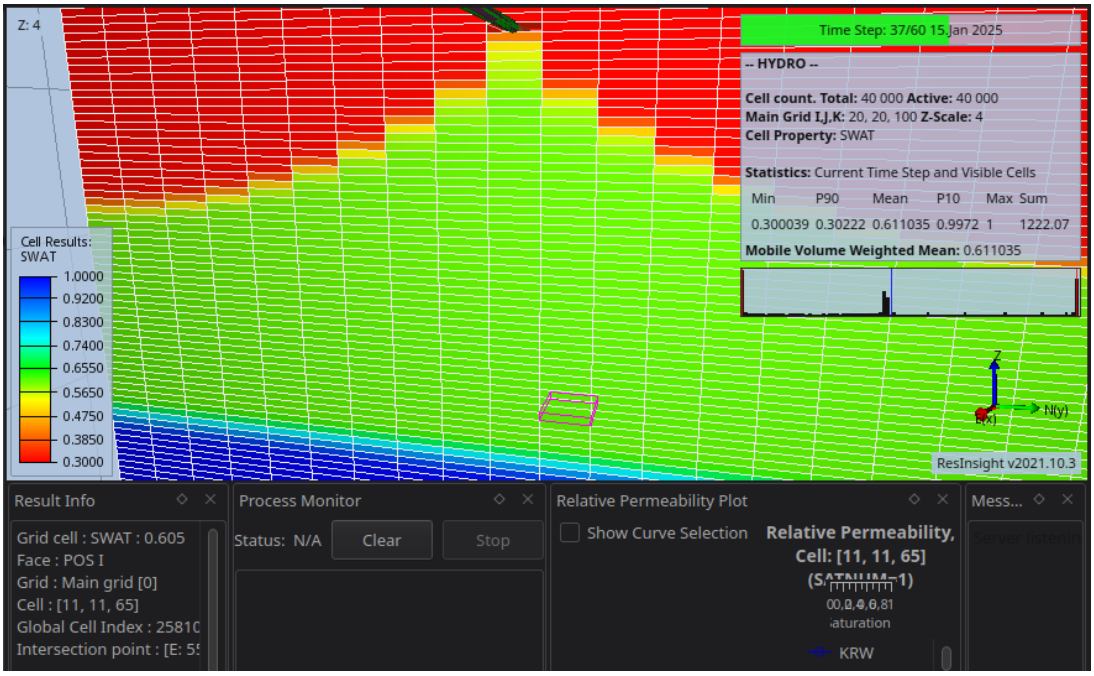

Figure 13: Actual position of water saturation equal to 1-Sor = 0.605 observed 90m down from the sensor.

Thus, it is already indicating that the further away the sensor is from the transition zone, the more inaccurate the estimate.

3.2 Changing Pc curves

In order to further study the results from above, varying transition zones were desired. Thus, the Pc curves in the input deck was modified such that the capillary pressure of interstitial water saturation of 0.3 was decreased to 0.7, then increased to 5, 10 and 100 respectively and run in 4 seperate runs. Water breakthrough for all four runs plus reference run in blue can be seen in figure 14. As expected, WBT happens earlier for the run with 100 Pc as the transition zone is higher and consequently there is both more water close to the well from the beginning of the run and down the column and water is produced earlier.

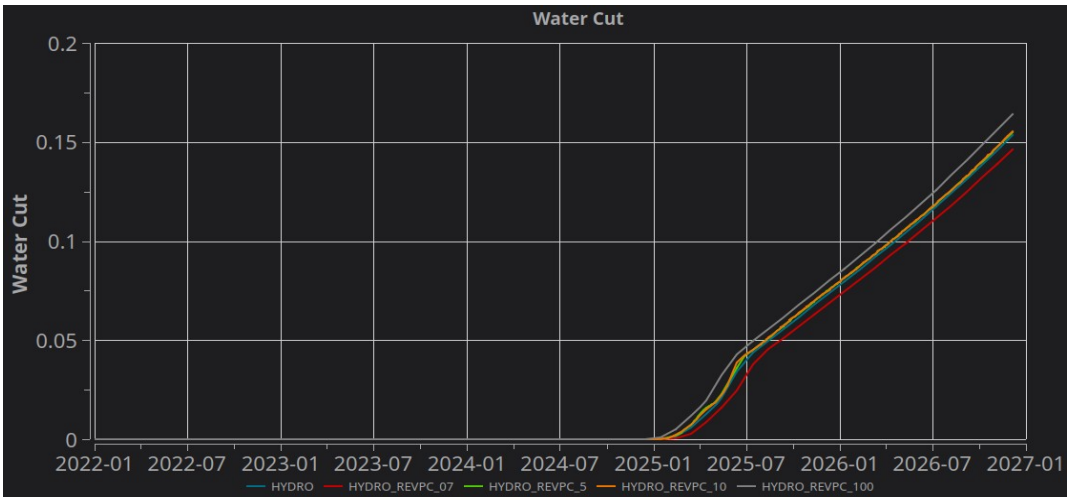

Figure 14: Field water cut for reference model and increasing Pc curves. Gray line indicates earlier WBT for the run with highest Pc curve and highest transition zone.

Also, the red line indicates the run with a shorter transition zone, and as expected, the WBT happens later than the other runs.

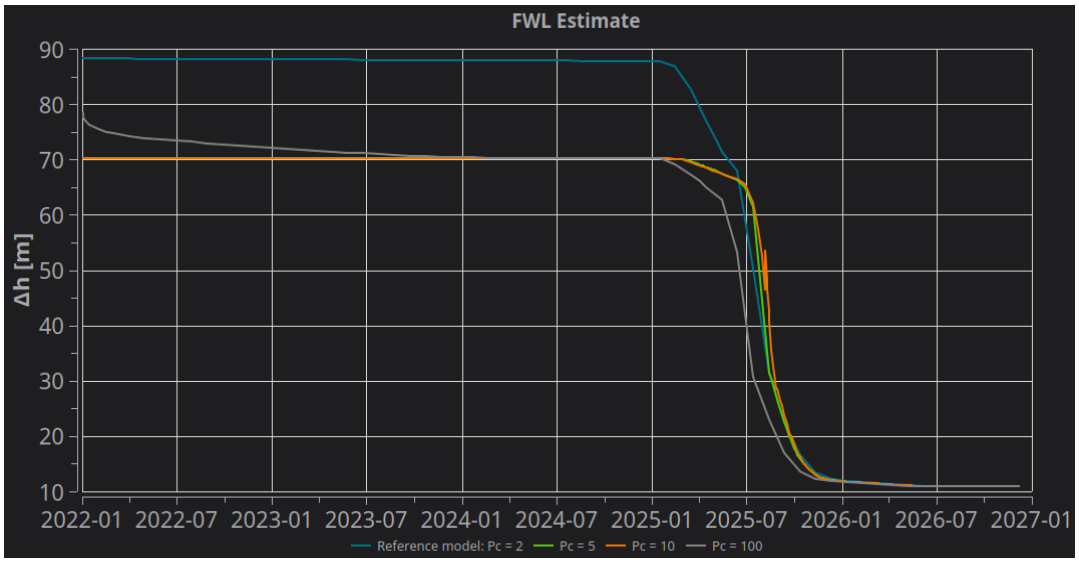

Figure 15: Δh for reference model and increasing Pc curves. Highest transition zone is achieved for the highest Pc indicated with a gray line.

When estimating FWL in these scenarios, we obtain the results seen in figure 22. Compared to the reference model (in blue), all other runs start with a distance to FWL lower than 88m.

This is expected as a higher transition zone should provide more water towards the sensor. However, both Pc = 5 and 10 are constant at 70m while Pc = 100 start at 78, then slowly decrease down to 70m and stay at 70m until WBT. It is difficult to explain this behavior. Also, it could be pointed out that for run with Pc = 10, the water saturation at block (11,11,20) was Sw = 0.3001 at the beginning of run while for the run with Pc = 100, the saturation at that block was Sw = 0.3099, indicating that the block is at a point further into the transtion zone, as it was supposed to be, yet Δh is higher for this run, indicating a longer distance down to the FWL initially. This should not be the case. This could be a result of the artificially inflated Pc curve at the endpoint as the yellow Pc-line in figure 8 would become an almost 90 degree curve.

3.3 Changing oil viscosity

To observe effects of more viscous oils, the oil viscosity at 621 bar was increased to 1, 5, 10 and 25 for 4 separate runs according to table 3.

Table 3: Values for reference model and 4 runs of increasing viscosities at their corresponding reference pressures.

	345 bar	621 bar
Reference run	0.449 cP	0.631 cP
Run 1	0.449 cP	1 cP
Run 2	1 cP	5 cP
Run 3	5 cP	10 cP
Run 4	15 cP	25 cP

Figure 16 shows change in water breakthough for reference model and the corresponding runs with increased oil viscosities. WBT happens earlier as viscosity is increased. This makes sense as viscous fingering becomes more prevalent and water will take the path of least resistance and reach the producer earlier and earlier.

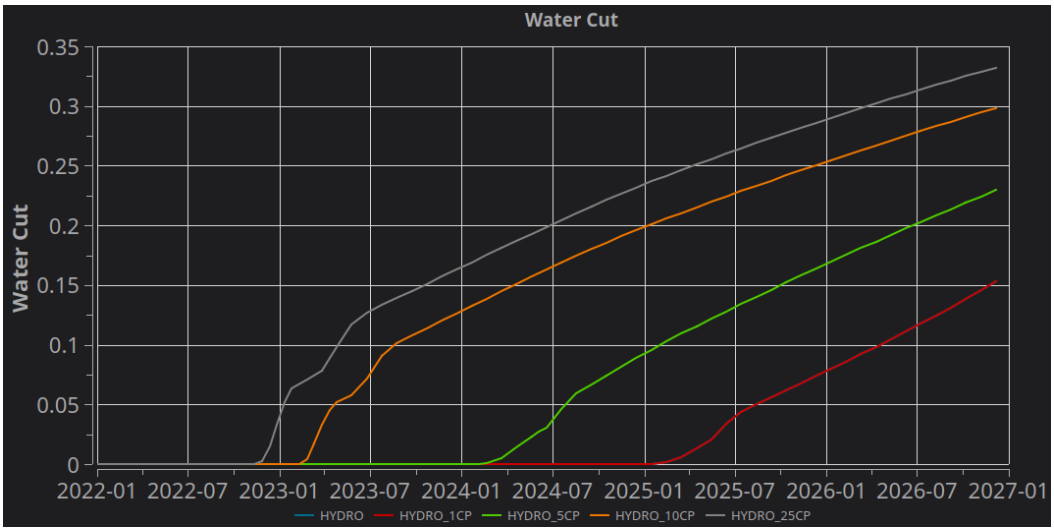

Figure 16: Field water cut for reference model and increasing oil viscosities. Earlier water breakthrough follows an increase in viscosity due to viscous fingering.

However, when estimating FWL with increasing oil viscosities, the run with 25cP is not the run to first indicate a rise in FWL.

As seen in figure 17, the run with 25cP registers an increase in FWL after the run with 10cP

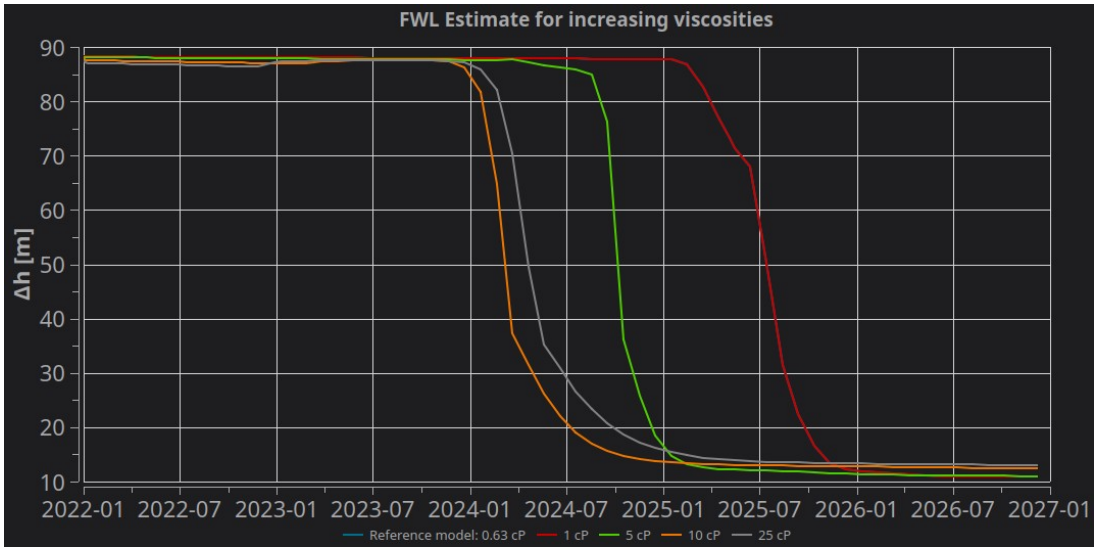

Figure 17: Estimate of FWL with increasing oil viscosities. The run with 25cP (gray) shows an increase in water level later than the run with 10cP (orange)

This is explained by looking at the I-slice in the 3D model as shown in figure 18. The distance down to the water front is impacted by the water cone effect from the viscous oil to such a degree that saturation changes (and thus changes in FWL estimate) is "squeezed" in towards the middle and down.

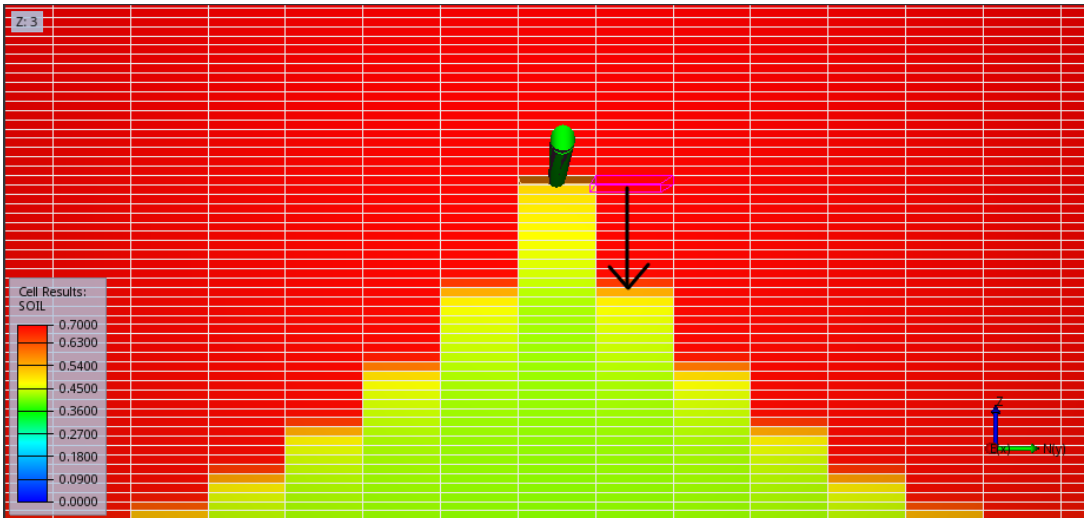

Figure 18: Water cone from high viscosity oil (25cP) at water breakthrough showing a larger cone effect.

Thus, although WBT happens earliest for the 25cP run, an FWL increase happens later for this run as the the viscous fingering effect has become the larger factor compared to the lower viscosity making saturation changes happen later. However, checking the actual distance to Sw = 1-Sor, we find this to be between block 68 and 69. Choosing block 68, this gives an FWL at 96 m which does not correspond to what is observed in figure 17. This shows that viscous fingering does not show up on the estimate for FWL as these fingers does not have high enough water saturation.

3.4 Thief zone

A thief zone is defined by Bane et al. (1994) as "*laterally continuous stratigraphic units of relatively high permeability which have approached residual oil saturation.*" In this thesis, the stratigraphic unit will not start with Sor, but rather approach Sor faster than the blocks around it. We have already seen effects of a water cone in chapter 3.3. However, in all of those scenarios, the water cone was directly underneath the well. Here, we artificially create a column of water that fills up faster than surrounding blocks, essentially creating a water cone effect positioned differently than above in order to observe the effects on FWL estimate. The thief zone was constructed such that the top 40 layers (80m) of the reservoir were of equal permeability of 200mD in the z direction (x- and y-direction same as reference at 256mD). Then, in layer 41, 700mD in z-direction was put into block (8,7,41) and all subsequent blocks directly beneath it. As the model had 100 layers, it now had a thief zone in blocks (8,7,41-100) (the X position). That is, the model now had a column of blocks from layer 41 to the bottom of the aquifer where the permeability was much higher than the surrounding blocks. For comparison, a separate run was done where the thief zone was moved to a position in the corner of the reservoir, in block (20,20,41-100) (Y position), furthest away from the first position in order observe any changes in the estimate of FWL. The position of the thief zones as seen from above is illustrated with an X and Y in figure 19 for first position and second position respectively.

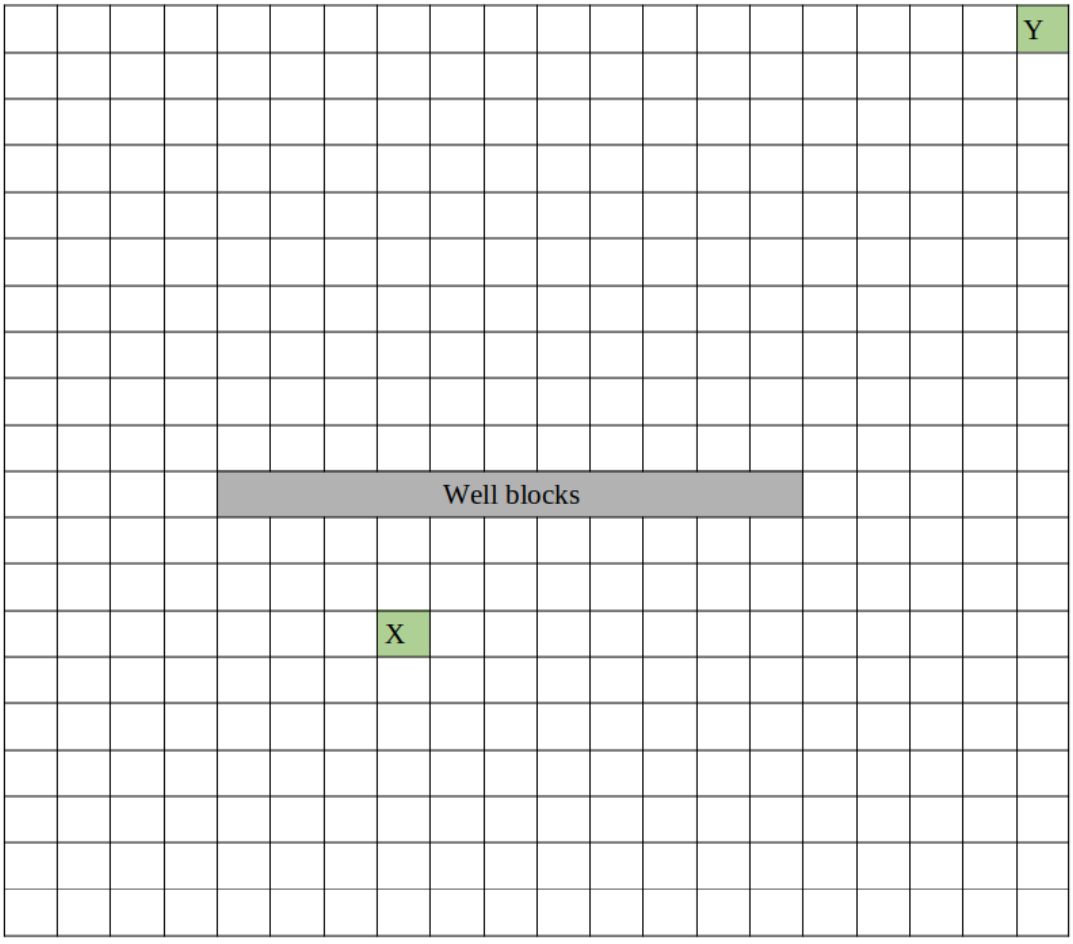

Figure 19: Illustration of thief zone position as seen from above. First position marked by X. Second position marked by Y.

Then, thief zone X was run again with a permeability column of 1500mD in order to fill the column with water faster than the first run, that is, to produce a more “pointy” water cone. As can be seen in figure 20, WBT happens earlier for the reference run, but at the same time for all thief zone runs. This is expected as the size of the thief zone is the same for all runs, and as

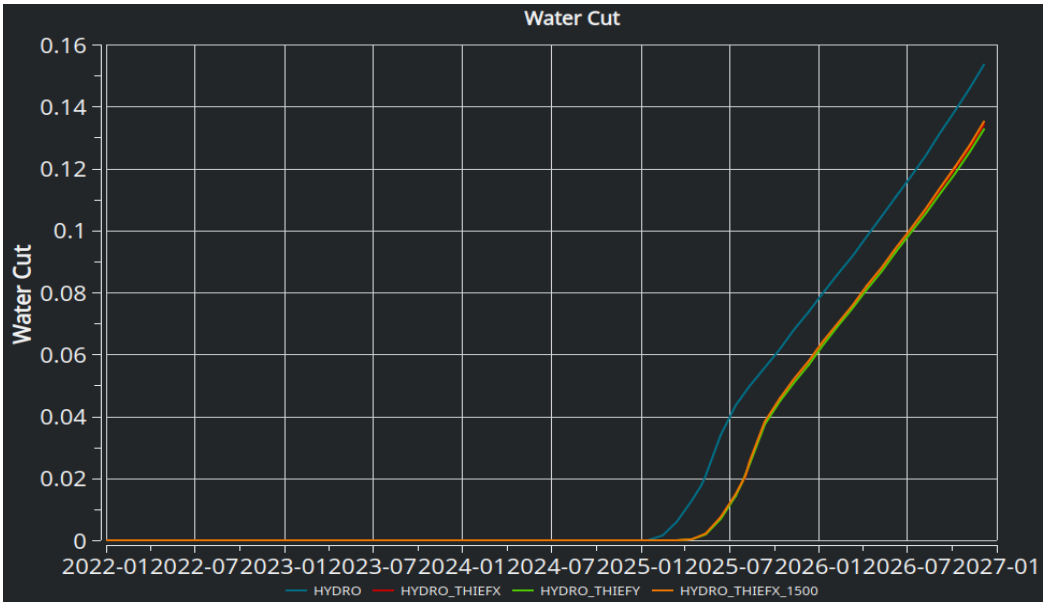

Figure 20: WBT for reference run and three separate thief zone runs. X, Y and X with 1500mD all have WBT at the same time.

long as the water influx from the aquifer remains the same for all runs, the time required to “trap” the water is the same, and WBT should be unchanged. However, as water escape into the thief zone, less water moves towards the producing well, and as such, all runs produce a WBT later than the reference model without theif zone.

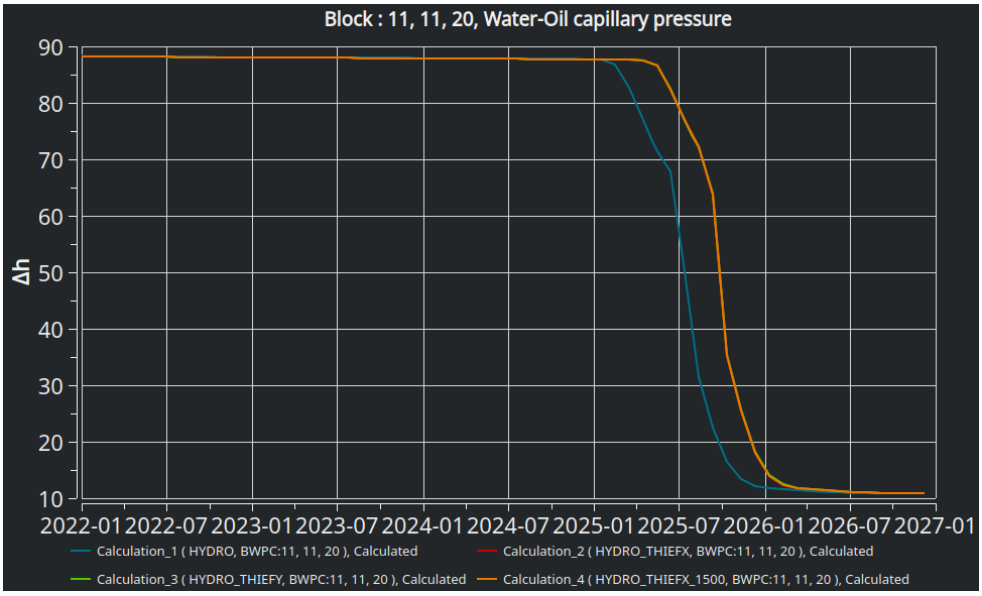

Figure 21: Δh for runs with thief zones. All thief zones show an increase in FWL at the same time.

Again, equation (4) was run for all four to produce the results seen in figure 21. Here it is observed that increase in water level is registered later than for the initial run for all thief-zone runs, while at the same time is almost identical for the three thief zone cases. This indicate

that it does not matter where in the reservoir the water column is rising. However, it is unexpected that the run in thief zone X with 1500 mD is the same as the first two runs. As the water colum rises faster for this run, an increase in FWL should be registered earlier here. However, it is possible it is not fast enough to make an impact on this scale. Another reason for this could be what we saw when we had viscous fingers, the saturation of these were not enough to have an impact on FWL readings, and as such, these thief zones may not be registered by the sensor at all. Looking at the 3D model for the 1500mD run, this is confirmed as shown in figure X. The highest point in the reservoir with a water saturation of 0.605 is found in the thief zone column in block (8,7,56) for 14th of July 2025, giving an actual FWL depth of 72 m. This is not completely accurate, yet not too far off what is observed in figure 21 which gives an estimate of around 78 m for that date.

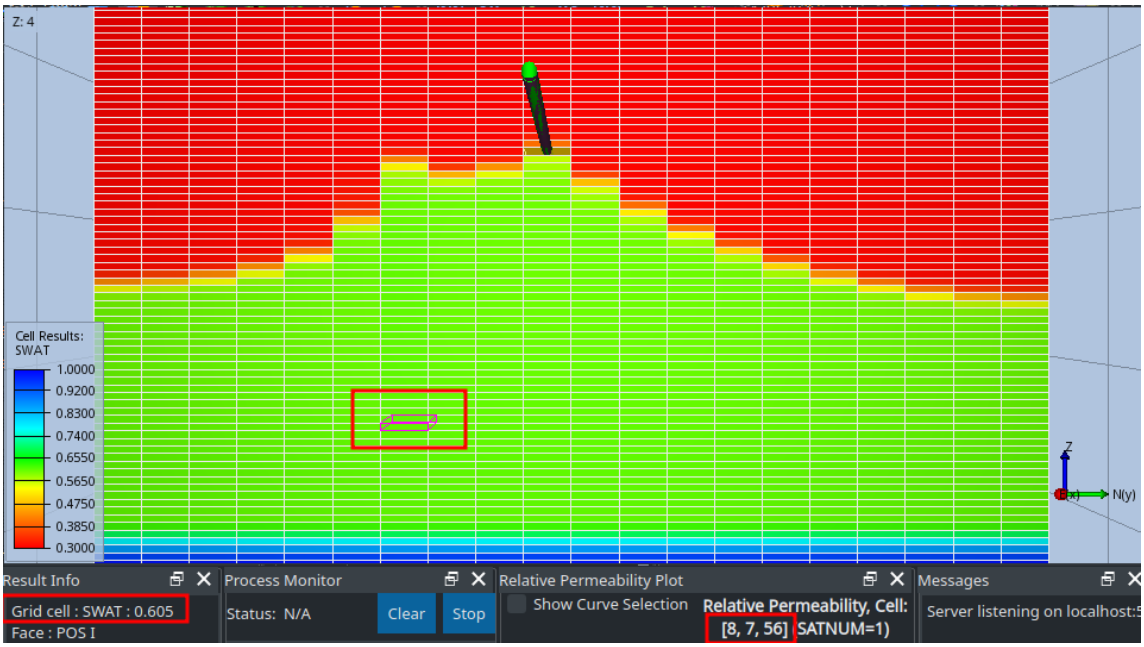

Figure 22: Water saturation in the thief zone X with 1500 mD on 14th July 2025, indicating a distance to FWL should be 72m.

3.5 Changing production rate

Changing the production rate would let us control the speed at which the water level rise in the reservoir as a whole in order to check if this has an impact on FWL readings. Rate of 500, 1500, 3000 (reference model) and 4500 sm3/day were run to produce the first two runs with no WBT and the last two with WBT as seen in figure 23.

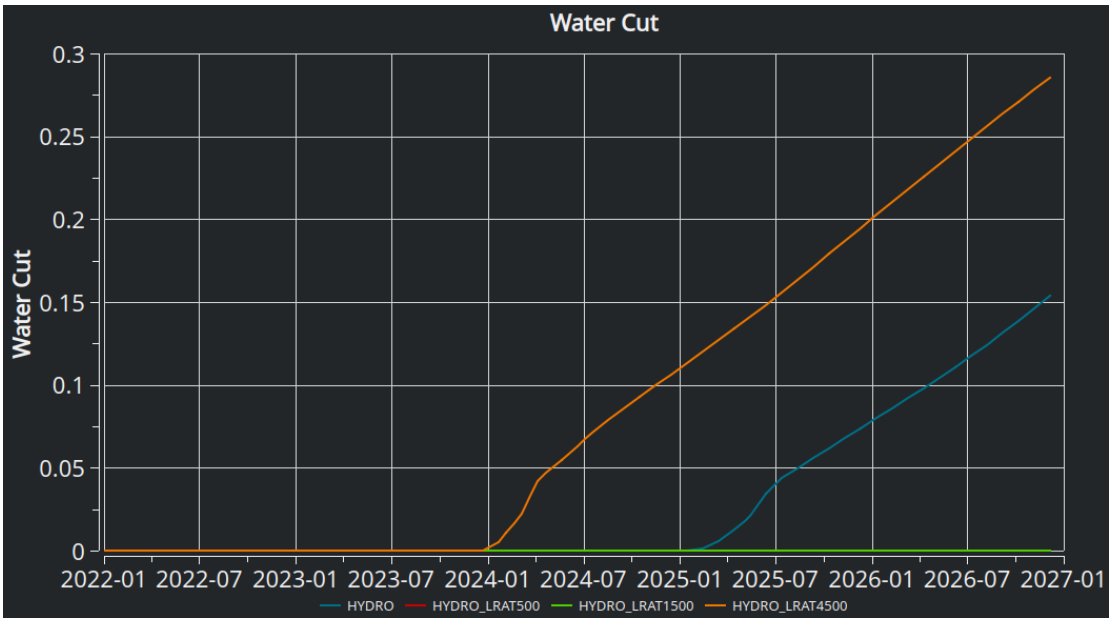

Figure 23: FWC for reference model and varying liquid production rates of 500, 1500, 3000 (reference model) and 4500 sm³/day. The former two shows no WBT while the latter shows an earlier WBT than the reference model.

The observations from figure 24 is as expected. The two runs without WBT hardly show sign of FWL increasing at all while the 4500 sm³/day run shows increase in FWL exactly one year earlier than reference run, on par with the observations from figure 23.

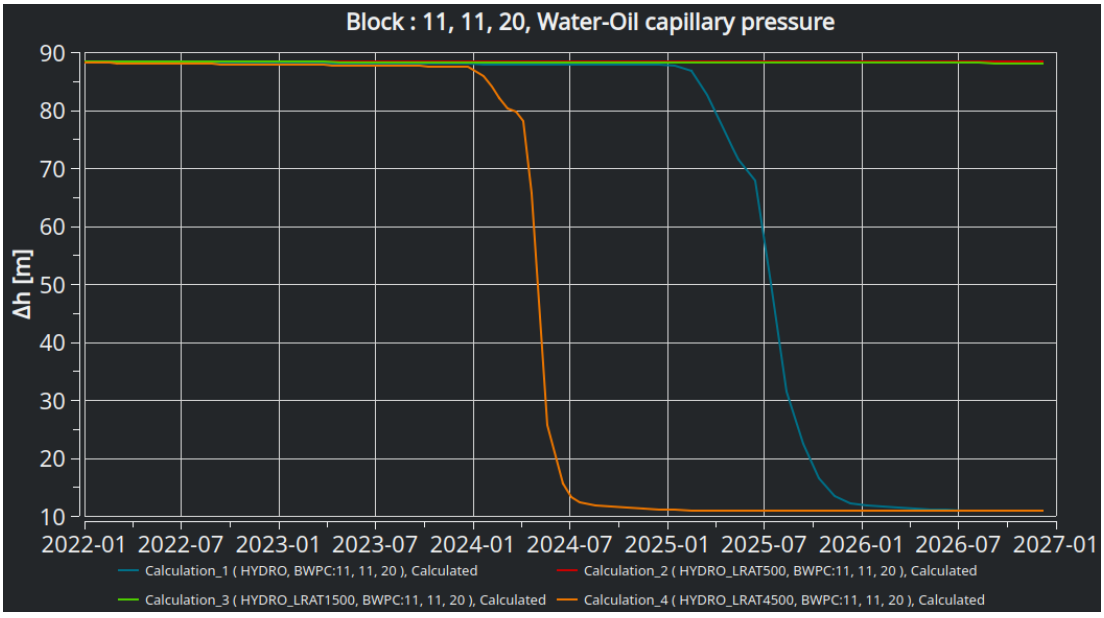

Figure 24: Distance to FWL for runs with varying liquid production rates. The run with 500 sm³/day show no change in FWL, while the run with 1500 sm³/day show only a slight sign towards the end of production.

The most noteworthy here is that the run with 1500 sm³/day seem to drop slighty more in Δh towards the end of production. According to Δh, FWL at that point should be 88m down from the sensor. Looking at the 3D model for this run, shown in figure 25, we see that block (11,11,64) has Sw = 0.605, meaning the FWL is exactly 88 m below the sensor at that point.

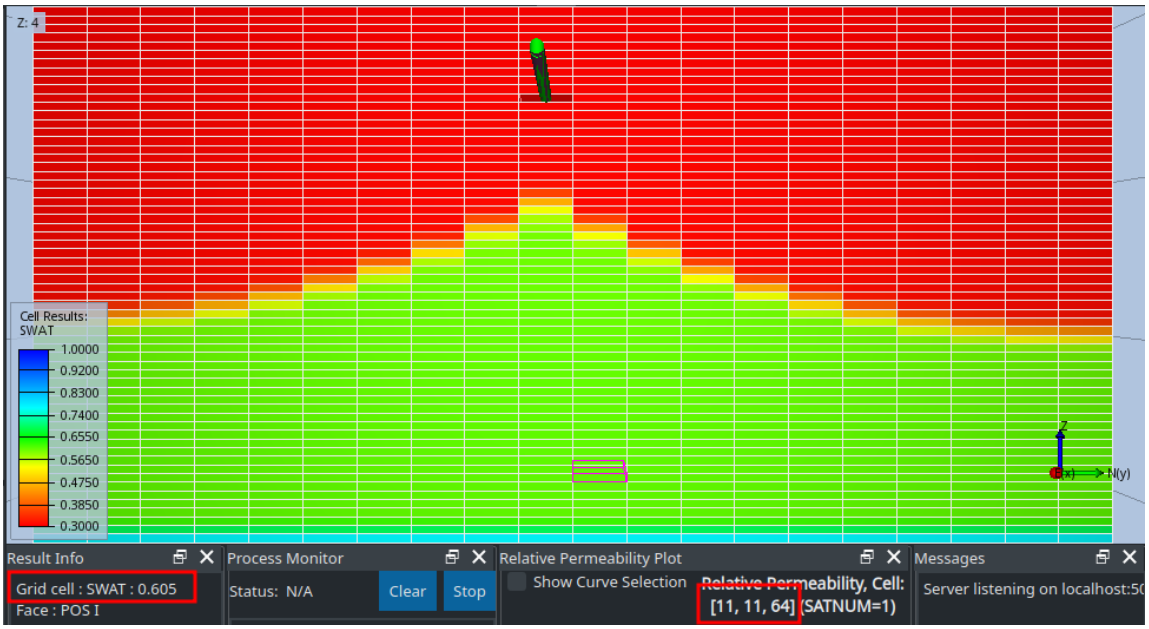

Figure 25: Actual distance to FWL at end of production for run with production rate of 1500 sm³/day. The water saturation of 0.605 is marked for cell (11,11,64).

This was also the saturation directly beneath the well, meaning this was indeed the highest point for FWL at that time. It is clear, that Δh and "real" distance in this scenario agree with each other for this dynamic scenario.

3.6 Shut-in of the well

Finally, a run was done where the well was shut-in after 1 year of production. This was done to observe if any change in FWL would be detected after 4 more years of shut-in. As expected only negligible amounts of water is produced until it goes to zero after 1 year of production as shown for FWC in figure 26.

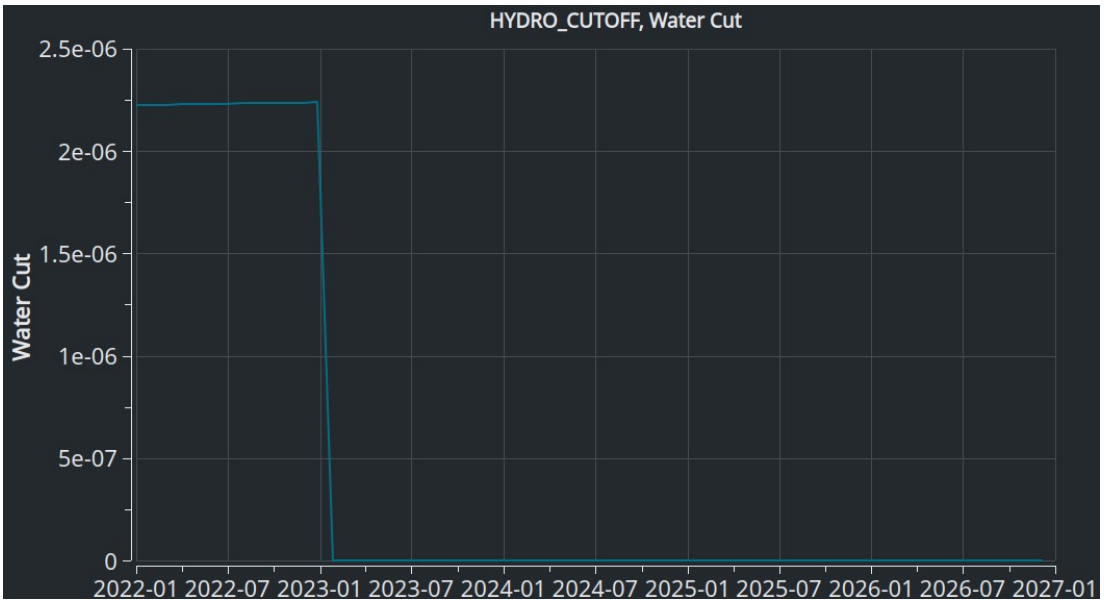

Figure 26: Field water cut for a well that is shut in after 1 year of production. Only negligible amounts are produced until it drops to zero.

In this case, as seen before, Δh starts by dropping slowly, indicating a rise in FWL, and then it jumps up to 88,4 m after the shut-in at 2023-01 as shown in figure 27.

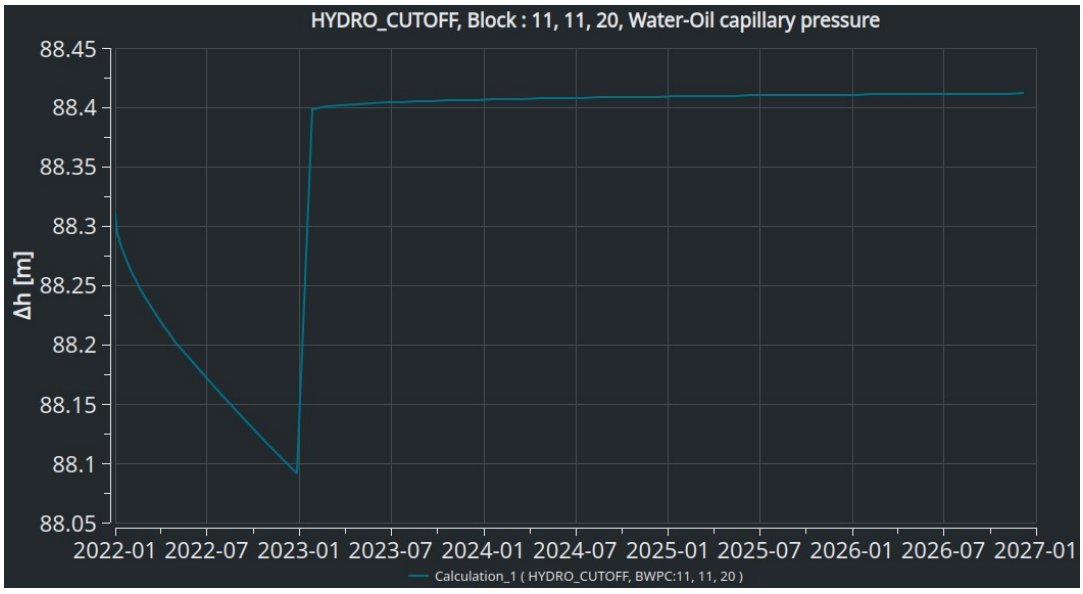

Figure 27: Distance to FWL for a well that is shut in after 1 year of production. The graph shows the water level receding slightly over 4 years after shut-in.

At Jan. 26th 2023, a water saturation of 0.605 was measured in cell (11,11,68), shown in figure 28, giving an actual FWL at 96 m below the sensor.

After 5 years, a water saturation of 0,605 was registered in cell (11,11,67), giving an actual distance from sensor down to FWL of 94 m. This means that after 4 years of shut-in, the FWL had actually risen by 2m (a smaller Δh), yet this was not picked up by the sensor who, on the contrary, detected the FWL falling (increasing Δh). This shows that the two definitions of "FWL is where Pc = 0" and "the point where water saturation has reached 1-Sor (the point where oil is no longer mobile)", will yield conflicting results in this scenario. Equation (4) which is used for Δh instantly picks up that the well is shut in, yet when the receding water cone as seen in figure 28 spreads out over the next 4 years, the equation shows the FWL is sinking on a scale of mm, not increasing 2 m.

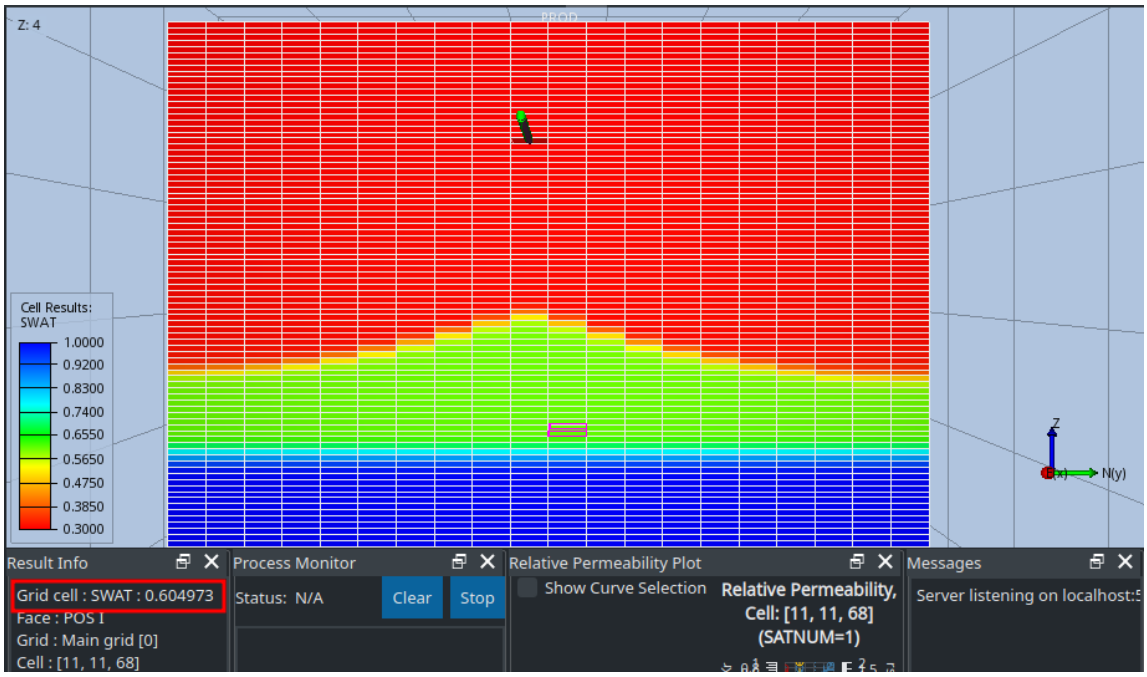

Figure 28: Actual distance to Sw = 1-Sor for column 11,11. Marked cell (11,11,68) is shown with Sw = 0.6049

This could be an indicator, that when water is receding in a static condition, it can take a longer time than 4 years to be picked up by the sensor.

4 Conclusion

Simulations were done in order to look into how pressure differences between oil and water in a water wet reservoir is influenced by various mechanisms. From this, we wanted to see how the free water level could be estimated in different scenarios. With this goal in mind, we first observed the effects of a reference model to use as a basis. Then, we observed effects from different capillary pressure profiles, oil viscosity , thief zones, production rates and effect from a well that is shut in.

It was found how saturation levels plays an important role in the estimation for the free water level. Unless there is a change in water saturation, the capillary pressure seems to be unchanged in all scenarios, leaving the distance to FWL in a constant position. This means that if the sensor is placed in a spot above the transition zone, this method will not detect any changes until oil saturation starts to decrease. As such, a higher transition zone led to a shorter distance to FWL, although these simulations also produced some inconclusive results. Moreover, we learned how columns of water, such as thief zones or viscous fingers would not be detected. As such, the FWL further down in the reservoir would be correctly estimated as further down, while the water breakthrough would not be seen in advance with the method used in this thesis.

However, we also saw how the positioning of the thief zones made no difference to the estimate of the FWL, meaning the distance would be correctly estimated even if the FWL is not directly beneath the sensor.

And lastly it was shown how receding water seemingly gave conflicting results where the estimate showed an increase in distance while what actually happened was a decrease in distance.

In closing, it should be pointed out that the reservoir used in the simulations are by no means a representation of a real reservoir. It is a relatively simple model with a purpose of isolating specific effects. Moreover, with hysteresis implemented, results would turn out differently and with the heavily modified Pc curves used in the model, it brings into question how reliable the results are. As such, the results from changing viscosity and thief zones are perhaps the most reliable ones as it clearly show how these zones and fingers are not detected with the method and definitions used in this thesis.

For future work I would recommend implementing hysteresis and increase time to see how it impacts the estimates and time required for FWL to become zero. Shut-ins over longer periods and series of shut-ins could be done to see if consistent results could be produced as the result obtained here is only indicative and not conclusive. Even further, a system containing gas is a highly relevant scenario to simulate in order to see how Hydrotells tool will respond to three phases instead of two.

References

AAPG, wiki. (2022a). *Determining fluid pressure from repeat formation testers*. https://wiki.aapg.org/Determining_formation_fluid_pressure_from_RFTs

AAPG, wiki. (2022b). *Formation fluid pressure from drill stem tests*. https://wiki.aapg.org/Determining_formation_fluid_pressure_from_DSTs

AAPG, wiki. (2022c). *Methods for obtaining formation fluid pressures*. https://wiki.aapg.org/Methods_for_obtaining_formation_fluid_pressures

Ahmed, PE, Tarek. (2019). *Reservoir Engineering Handbook*. San Diego: Elsevier Science & Technology.

Ahmed, T. (2010). *Reservoir Engineering Handbook*. Elsevier.

Ahmed, T., & McKinney, P. D. (2005). *Advanced Reservoir Engineering*. Elsevier.

Andersen, P. Ø. (2021). *Analytical modeling and correction of steady state relative permeability experiments with capillary end effects – An improved intercept method, scaling and general capillary numbers*. https://doi.org/10.2516/ogst/2021045

Bane, R. K., Parker, R. A., Storbeck, W. G., & Sunde, R. L. (1994). *Reservoir Management of the Fullerton Clearfork Unit*., SPE-27640-MS. https://doi.org/10.2118/27640-MS

Baxendale, D. (2021). *OPM Flow Reference Manual*. OPM-OP AS. https://opm-project.org/?page_id=955

Capotosto, A., Lopes, B. de C. F. L., & Tarantino, A. (2021). *Proof-of-concept for a probe to measure pore water pressure in oil-water saturated porous rock*. Journal of Petroleum Science and Engineering, 198, 108183. https://doi.org/10.1016/j.petrol.2020.108183

Dolan, J. P., Einarsen, C. A., & Hill, G. A. (1957). *Special Applications of Drill-Stem Test Pressure Data*. Transactions of the AIME, 210(01), 318–324. https://doi.org/10.2118/851-G

Elshahawi, H., Fathy, K., & Hiekal, S. (1999). *Capillary Pressure and Rock Wettability Effects on Wireline Formation Tester Measurements*. SPE-56712-MS. https://doi.org/10.2118/56712-MS

Fetkovich, M. J. (1971). *A Simplified Approach to Water Influx Calculations-Finite Aquifer Systems*. Journal of Petroleum Technology, 23(07), 814–828. https://doi.org/10.2118/2603-PA

Hoyer, C., Fried, S., & Sask, D. (1996). *Test, Treat, Test System Using a Concentric Coiled Tubing/DST Package*. PETSOC-96-77. https://doi.org/10.2118/96-77

Khan, M. I., & Islam, M. R. (2007). Reservoir Engineering and Secondary Recovery. In M. I. Khan & M. R. Islam (Eds.), *The Petroleum Engineering Handbook: Sustainable Operations* (pp. 189–241). Gulf Publishing Company. https://doi.org/10.1016/B978-1-933762-12-8.50013-1

Kleppe, J., & Morse, R. A. (1974). *Oil Product from Fractured Reservoirs by Water Displacement*. Society of Petroleum Engineers of AIME.

Lake, L. W. (1989). *Enhanced oil recovery*. Prentice Hall.

Leverett, M. C. (1941). *Capillary Behavior in Porous Solids*. Transactions of the AIME, 142(01), 152–169. https://doi.org/10.2118/941152-G

Niculescu, B. M., & Ciuperca, C. L. (2019). *Identification of fluid contacts by using formation pressure data and geophysical well logs*. In 19th International Multidisciplinary Scientific GeoConference SGEM 2019 (Vol. 19, Issue 1.2, pp. 897–908). STEF92 Technology. https://doi.org/10.5593/sgem2019/1.2/S06.114

Nygård, J. I., & Andersen, P. Ø. (2020). *Simulation of Immiscible Water-Alternating-Gas Injection in a Stratified Reservoir: Performance Characterization Using a New Dimensionless Number*. SPE Journal, *25*(04), 1711–1728. https://doi.org/10.2118/200479-PA

Rasmussen, A., Sandve, T. H., Bao, K., Lauser, A., Hove, J., Skaflestad, B., Klöfkorn, R., Blatt, M., Rustad, A. B., Sævareid, O., Lie, K.-N., & Thune, A. (2021). *The Open Porous Media Flow reservoir simulator*. Development and Application of Open-Source Software for Problems with Numerical PDEs, *81*, 159–185. https://doi.org/10.1016/j.camwa.2020.05.014

Rolfsvåg, T. A., Lindsay, C., Zuta, J., Vatne, K. O., Lohne, A., Iversen, J. E., Guo, Y., Askarinezhad, R., Undheim, E., Gudmestad, T., & Bye, A. (2019). *Water Pressure Measurement Inside a Hydrocarbon Column*. D011S006R002. https://doi.org/10.2118/195639-MS

Schlumberger. (2014). *Eclipse Technical Description*. Schlumberger.

Schlumberger. (2022). *Buildup test*. https://glossary.oilfield.slb.com/en/terms/b/buildup_test

Soliman, M. Y., Petak, K., Christensen, J., & Centanni, R. (1988). *Analysis Of Sequential Formation Testing And Surge Tests Using New Techniques*. PETSOC-88-39-53. https://doi.org/10.2118/88-39-53